UNIVERSITÀ DI PADOVA  FACOLTÀ DI INGEGNERIA

DIPARTIMENTO DI INGEGNERIA DELL'INFORMAZIONE

Corso di Laurea Magistrale in Bioingegneria

Tesi di Laurea

ANALYSIS OF TRANSIENT FAILURES IN CONTINUOUS GLUCOSE MONITORING SENSORS: DATA MODELING AND SIMULATION

Relatore: Prof. Giovanni Sparacino

Correlatori: Dott. Ing. Simone Del Favero

Dott. Ing. Andrea Facchinetti

Laureanda: Alessandra Khoury

Anno accademico 2011/2012

Padova, 23 Aprile 2012

A mamma, papà

Contents

SOMMARIO

Una delle più promettenti recenti innovazioni tecnologiche nella terapia del diabete sono i dispositivi per il monitoraggio quasi continuo della glicemia (CGM). Questi piccoli sensori sottocutanei rendono disponibile una grande mole di dati, prima inacessibile, il cui utilizzo consente a paziente e diabetologo di migliorare significativamente la qualità del controllo glicemica. Questa tecnologia ha rinnovato l'intresse verso l'implementazione di un dispositivo per il controllo automatico in catena chiusa della glicemia (Pancras Artificiale), che grazie ad essa può diventare finalmente portatile e minimamente invasivo.

Un'altra tecnologia chiave nel campo per lo sviluppo del Pancreas Aritficiale è il simulatore del paziente diabetico, uno strumento software che consente di evitare i lunghi e dispendiosi trial sugli animali, una volta necessari prima di testare un dispositivo sugli esseri umani.
Visto il ruolo sempre più cruciale delle simulazioni in questo settore, è importante poter includere in queste gli errori ed i faults a cui sono soggetti i dispositivi CGM così da testare la robustezza degli algoritmi a questi eventi e la loro efficacia nel gestirli.

Questa tesi si propone di rispondere alla necessità di modelli per gli errori e i faults che comunemente si riscontrano nei dati CGM reali, da utilizzare nei test simulati di robustezza.

Dall'osservazione di un data set fornito da misure con sensori CGM Dexcom® (Capitolo 2) sono stati individuate tre classi di errori e per ciascuna di queste è stato proposto un modello e un modulo di simulazione. Le *disconnessioni* (Capitolo 3) consistono nella perdita di almeno un campione, a causa di un malfunzionamento della comunicazione tra i componenti trasmissivi e ricettivi del sensore. Un modello di Markov a due stati è stato proposto e validato. Gli errori di tipo *segnale non valido* (Capitolo 4) sono stati associati all'indicazione del ricevitore pari a 9 o 10 mg/dl. Per questo tipo di errore un modello di Markov a due stati non è stato sufficiente a descrivere l'intera casistica, che comprende errori di breve durata (meno di un'ora) e di lunga durata (alcune ore). Infine, un terzo tipo di errore è assimilabile ad una *perdita di sensitività* del sensore, a causa di una pressione sullo stesso. Il modello proposto e validato (Capitolo 5) consiste nell'assimilare tale errore ad una funzione gradino filtrato da un sistema dinamico del

primo ordine.

Per gli errori di disconnessione e di perdita di sensitività è stato possibile quindi proporre due moduli di simulazione che permettono di avvicinare i profili glicemici simulati a quelli ottenuti da misurazioni reali con sensori CGM; nel caso degli errori di tipo 'segnale non valido' la simulazione è stata avviata sfruttando l'informazione statistica empirica dei dati (Capitolo 6).

SUMMARY

One of the most promising recent technological innovation in diabetes management are the devices for continuous glucose monitoring (CGM). These small subcutaneous sensors give us a large amount of information that was inaccessible before. Using these sensors allows both patient and diabetologist to significantly improve the quality of the closed loop control of glycemic levels. This technology has renewed the interest in the development of a device for closed loop automatic control of glycemia (Artificial Pancreas), that can eventually be wearable and minimally invasive.

Another key technology for the Artificial Pancreas development is the physiological simulator of a diabetic patient, a software tool that allows to avoid expensive and time consuming trials on animals, that once were necessary in order to test any device for human beings.
Since simulation is becoming more and more crucial in this field, it is important to involve the most common failures that affects CGM devices, so that algorithms' robustness to these events can be tested together with their skill in managing them.

This thesis is meant to meet the need for models of the most common failures which can be used for robustness simulated tests.

The observation of a data set of Dexcom® CGM measurements (Chapter 2) led us to identify three kinds of failures and for each one of them a model was proposed. *Disconnections* consists of the loss of at least one sample, caused by the interruption of communications between transmitter and receiver. A two-state Markov model was proposed and validated. *Invalid Outputs* (Chapter 4) were associated with the received CGM readings of 9 or 10 mg/dl. In this case, the two-state Markov model was not suitable for the description of both short (less than one hour) and long-lasting (several hours) failures. Lastly, a third kind of failure was classified as a *loss of sensitivity* of the sensor, caused by a pressure on the sensor itself. The model, that was proposed and validated (Chapter 5), described this failure as a step function filtered by a first order system. For what concerns disconnections and losses of sensitivity we could build simulation tools that allow us to make simulated glyceimic profiles more similar to the real ones. In order to simulate

invalid outputs, the simulation was run with the empirical statistical information (Chapter 6).

1

Diabetes and Continuous Glucose Monitoring

Diabetes Mellitus is a metabolic disease characterized by either the insufficient production of the insulin hormon to maintain the glucose level in the normal range (Type-1 diabetes), which is usually set between 70 and 180 mg/dl, or the inability of the body to respond to the insulin formed within the system (Type-2 diabetes). To cover this deficiency, conventional approach is to introduce insulin with subcutaneous injections. In order to determine the proper dosage for their insulin injections patients have to frequently monitor their blood glucose concentration by means of Self Monitoring Blood Glucose (SMBG) therapy (i.e. 3-4 finger stick measurements per day). In the last few years new sensors have been developed, allowing Continuous Glucose Monitoring (CGM), e.g. a glucose measurement is obtained every 5 minutes and for several days. These devices significantly improve diabetes management detecting more critical episodes (i.e. hypo and hyperglycemia) rather than conventional SMBG.
In this chapter Diabetes and related complications, SMBG and devices for CGM will be briefly introduced and described.

1.1 Diabetes Pathophysiology

Glucose is the main power source for the organism, and its concentration in blood circulation is characterized by a dynamic equilibrium between its production and utilization.

Normally, the organism receives the amount of glucose he needs from food, while liver and kidneys supply it in case of short fasting. In a healthy person, glycemia is accurately regulated by the organism, and insulin, produced by pancreas, is the crucial hormon in glucose metabolism. Diabetes is a chronic disease that occurs either when the pancreas does not produce enough insulin or when the body cannot effectively use the insulin it produces. Hyperglycaemia, or raised blood sugar, is a common effect of uncontrolled diabetes and over time leads to serious damage to many of the body's systems, especially the nerves and blood vessels.

Diabetes is classified into two types:

1. *Type-1 diabetes mellitus (T1DM)*: previously known as insulin-dependent, juvenile or childhood-onset, is characterized by deficient insulin production and requires daily administration of insulin. The cause of type 1 diabetes is not known and it is not preventable with current knowledge.

   Symptoms include excessive excretion of urine (polyuria), thirst (polydipsia), constant hunger, weight loss, vision changes and fatigue. These symptoms may occur suddenly.

2. *Type-2 diabetes mellitus (T2DM)*: formerly called non-insulin-dependent or adult-onset, results from the body's ineffective use of insulin. Type 2 diabetes comprises 90% of people with diabetes around the world, and is largely the result of excess body weight and physical inactivity.

   Symptoms may be similar to those of Type 1 diabetes, but are often less marked. As a result, the disease may be diagnosed several years after onset, once complications have already arisen. Until recently, this type of diabetes was seen only in adults but it is now also occurring in children.

1.2 Glucose monitoring and Diabetes Therapy

Diabetes therapy's aim is that of keeping glucose levels in the euglycemic range (70-180 mg/dl), so as to minimize or at least delay diabetes complications: over time, diabetes can damage the heart, blood vessels, eyes, kidneys and nerves. At present, diabetes conventional therapy relies on insulin and drug administration, diet and physical exercise: people with T1DM require insulin, while people with T2DM may not need it and can be treated with oral medication. Until the fifties insulin dosage was determined without considering real glucose levels of the patient. Setting insulin dosage is a challenging subject, and starting from the eighties this decision was up to new devices and technologies that could help Self Monitoring Blood Glucose (SMBG).

A typical SMBG test includes a drop of blood, obtained via a finger prick and applied to a chemically treated reagent strip, which is analyzed by the device. The test provides discrete and highly accurate data about current blood glucose levels. Insulin administrations rely then on three or four measures of blood glucose level per day: accuracy of the therapy is user-dependent, i.e. patients should be taught how to modify their food intake and therapy according to the SMBG data and in order to realize their individual glycemic goals. The insulin therapy then can

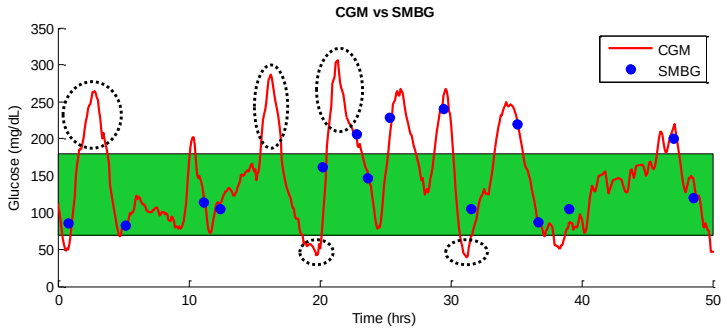

Figure 1.1 *Comparison between CGM data (red profile) and SMBG measurements (blue dots). The green area shows the normal range of blood glucose.*

be administered in two ways:

Multiple injection regimen: multiple daily subcutaneous injection are perfomed with syringes. Injection sites are the tissue of the upper arm and the anterior and lateral aspects of the thigh, buttocks, and abdomen. *Short acting* insulin should be injected within 30 min before a meal or immediately after a meal, in order to oppose the quick rise of the glycemic level due to the food intake, while *Long acting* insulin are administered to provide a basal insulinemia.

Continuous subcutaneous insulin infusion (CSII): a subcutaneous infusion pump injects of *short acting* insulin, delivered via a needle or a catheter sited under the skin and connected to a reservoir of insulin and a command module. This therapy is aimed at replacing *long acting* insulin for basal needs, continuously delivering *short acting* micro boli of insulin. However, insulin pumps are expensive, and at present they are available to a little amount of patients.

Nonetheless, the few SMBG samples do not give us enough information about critical glycemic episodes, e.g postprandial hypoglycemia and hyperglycemia. We find an example of this drawback in Figure 1.1. The several SMBG measurements performed (blue dots) could not catch three episodes of severe hyperglycemia and two of mild hypoglycemia, which are instead highlighted by the real glycemia data (red profile) and its excursions outside the range of normal glucose level (green area).

The SMBG inefficiency to identify all glucose excursions out of the euglycemic range, together with the pain associated with finger pricking, led during the last decade to the de-

velopment of new electronic devices that allow a quasi-continuous and minimally-invasive measurement of blood glucose concentrations, the so-called Continuous Glucose Monitoring (CGM) wearable systems. CGM measurements provide relevant information about the diabetes of a patient, and the importance of this technology will be discussed in Section 1.3.3, together with its drawbacks.

1.3 CGM sensors

Continuous glucose monitoring systems are electronic devices that measure physiological glucose levels. Glucose readings are provided every 1 to 5 minutes for several days (up to 7 days). Usually the device is made of a glucose sensor, that measures glucose levels of blood or interstitial fluid, and a wireless (or wired) transmitter which communicates glucose readings to a receiver that displays the current glucose data. CGM devices enable the identification of the overall trend in the glucose level, and based on these trends, proximal glucose levels can be forecast, along with hypo and hyperglycemia. The retrospective analysis of CGM direction, frequency and magnitude supply trend information that assists in optimizing treatment plans, adapting insulin regimens and facilitating clinical decisions.

Depending on the placement of the glucose sensor, we can define the degree of invasiveness of a CGM device. From this point of view, they can be classified into two groups: minimally-invasive and non-invasive devices.

1.3.1 Minimally-Invasive Devices

The minimally-invasive technologies measure glucose concentrations in the subcutaneous tissue, where the sensor is partially sited. Hence this classification describes the fact that the measurement does not draw from any blood vessel, but yet it compromises the skin barrier. This type of CGM systems is usually made of two components: a subcutaneous glucose sensor implanted on patient's skin, which provides measurements of the interstitial glucose concentration and is also a transmitter, and a small device that receives, stores and visualizes CGM data.

The subcutaneous sensor can be based on different principles, e.g. microneedle technology is made of silicon micro-needles that penetrate the skin and draw small samples of blood, while micropore technology employs laser ablation to create microscopic holes on the outmost layer

of the epidermis and draws interstitial fluid samples with a small local vacuum (for a complete review of current technologies see [2]). From a glucose detection technology point of view, most of the minimally-invasive sensors exploit a glucose-oxidase reaction to measure a raw signal, proportional to the glucose concentration of the site in which the biosensor is sited, i.e. in this case the interstitial tissue. This signal is usually a current given in mA. In order to read glucose leveles in mg/dl, a calibration procedure is then to be performed, using one or more SMBG samples. Some of the most important minimally-invasive CGM devices are:

- CGM System Gold (CGMS® System Gold™ Medtronic MiniMed, Northridge, CA, USA), FDA approved in March 2001 [19];
- GlucoDay® (A. Menarini Diagnostics, Florence, Italy), which received CE mark in Europe [20];
- Guardian® Real-Time (Medtronic MiniMed, Northridge, CA, USA), FDA approved in June 2005 [21];
- FreeStyle Navigator™ (Abbott Laboratories, Alameda, CA, USA), FDA approved in March 2008 [22];
- Seven® Plus (DexCom, San Diego, CA, USA), FDA approved in February 2009 [23]

The DexCom® Seven® Plus CGM system, which provided the data we analyzed in this thesis, will be talked out in Section 1.4.

1.3.2 Non-Invasive Devices

The need to avoid wounds and risk of infection from penetrating the skin has led to the challenging development of non-invasive sensors that measure glucose concentration from external body fluids assesment, such as saliva and tears [5], or with transdermal sensor based on optical approach. Focusing on the latter, the exploited detection technologies can involve fluorophores and thus measure Forster Resonance Energy Transfer (FRET) lifetime or intensity. Other optical techniques that do not use glucose-binding-fluorophore are e.g. Near Infrared (NIR) kromoscopy, Raman spectroscopy, polarimetry, photoacoustic spectroscopy and optical coherence tomography.

This kind of glucose monitoring is very promising, yet it will require several years before

reaching the market place. This is mainly due to many drawbacks concerning accuracy, precision and selectivity, i.e. the ability of the sensor to respond only to changes in glucose within the pool of molecules present in the body, like albumin and ascorbic acid.

Hereafter some intersting non-invasive sensors are briefly discussed:

- The NBM (OrSense Ltd., Nes Ziona, Israel) device is a prototype, and is based on occlusion spectroscopy [3]. The measurement is performed using an annular probe, which is positioned on the finger's root. The probe contains light sources and detectors operating in the red/near-infrared (RNIR) spectral region and pneumatic cuffs that produce oversystolic pressure to occlude blood flow. The occlusion of blood flow generates a dynamic optical signal, which facilitates accurate glucose monitoring. The technology is based on the direct effect of glucose on the scattering properties of the organ. Glucose decreases the mismatch in refractive index between scatterers and their surrounding media, leading to a smaller scattering coefficient and, consequently, a shorter optical path. As a result, with the growing concentration of glucose, fewer photons are absorbed and the light intensity increases. Development of this device is focused on improving the performance and ease of use in the home-use setting.

- The Solianis Multisensor (Biovotion AG, Zürich, CH) device uses impedance spectroscopy in order to measure glucose levels [4, 18]. The principle of glucose detection using this technology is: an increase in the local glucose concentration results in a decrease in the sodium levels and an increase in the potassium levels of the plasma, changing the dielectric strength, permittivity and conductivity of the plasma.

- The HG1-c nCGM (C8 MediSensors Inc., San Jose, CA, USA) is an investigational device, not cleared or approved for marketing in any jurisdiction [24]. This non-invasive CGM uses a light-sensitive sensor when detecting body's glucose levels and sends glucose measurements to a smart phone or any other compatible display device. It exploits Raman spectroscopy: the colours generated by Raman scattering, induced by illumination of a sample, are very specific to the exact chemical structure of molecules in the sample. Since glucose has its unique spectral fingerprint, it can be non-invasively measured beneath the skin.

1.3.3 Pros and Cons of CGM Devices

CGM devices have the great advantage to supply to both clinicians and diabetic patients a more complete information about the glycemic profile rather than SMBG. The possibility to have real-time information about the glycemic level and its trend is very useful in the management of patient's therapy, e.g. in the adjustment of the diet and the insulin dosage. Another significant improvement in diabetes management is also represented by the embedding in many of the CGM system of a tool able to generate visual and acoustic alerts when glucose concentration exceeds the normal range thresholds.
The portability of these devices and the possibility to receive an alarm when some fixed glycemic thresholds have been crossed, allow the diabetic patient to become more self-sufficient in the management of both therapy and critical events, e.g. post-prandial hyperglycemia and nocturnal hypoglycemia.

It is also important to remind that, nowadays, none of the CGM devices has been approved to substitute SMBG as reference in both control and management of the therapy. This fact is principally due to the lack of accuracy of CGM readings, accuracy which is crucial for the correct working of such a devices. Another critical topic with all CGM systems is calibration, i.e. relying on the glucose signal measured in interstitial fluid to blood glucose by means of capillary blood glucose measurements. For instance, if this is performed while blood glucose changes rapidly or if this is not performed with sufficient frequency to compensate for drift, there might be an unnecessary difference between measured and real glucose levels.

1.4 Dexcom® SEVEN® PLUS

The SEVEN® PLUS CGM System is a glucose-monitoring device for detecting glucose trends in adults with diabetes, and it is not approved for use on people aged less than 18, pregnant women or people on dialysis. The system received FDA approval for up to 7 days of use, although it is not designed to replace standard home glucose monitoring devices. Its use is helpful in order to detect hypoglycemic events, since it emits an alarm if the measured concentration of glucose reaches or goes under 55 mg/dl. The performances of the sensor were evaluated only for one probe insertion site, which is the skin of the abdomen [23].

Figure 1.2 *Components of the SEVEN® PLUS System: on the left the Receiver,a cell-phone sized device programmed to collect and process data from the sensor and to display the results as a glucose values, in the middle the Sensor with the Transmitter, on the right the Sensor with the applicator, used to insert the probe underneath the skin.*

1.4.1 System components

The SEVEN® system consists of three major components.

1. The Sensor, sterilized by electron beam and made up of three parts

   - Applicator: a disposable piece of the Sensor that you use to insert the Sensor Probe. There is a needle inside the Applicator that is removed once the Sensor Probe is inserted underneath the skin.
   - Sensor Probe: is the portion of the sensor that is actually inserted under the skin and measures glucose levels of the interstitial fluid in the sorroundings of the area in which it is inserted.
   - Sensor Pod: it sticks to the abdomen and holds the Transmitter in place. The Sensor Pod and the Transmitter are the only components that are actually worn by the patient during the glucose monitoring session.

2. The Transmitter, which snaps into the Sensor Pod and wirelessly sends glucose data to the Receiver.

3. The Receiver, a cell-phone sized device programmed to collect and process data from the Sensor and to display the results as a glucose value. Values above 400 mg/dl or below 39 mg/dl are not shown by the display.

1.4.2 Principle of operation

The SEVEN® PLUS Sensor exploits an electrochemical reaction with glucose. The reagent used is glucose oxidase, obtained from a microorganism, and less than 0.4 µg is applied to each Sensor Probe (for a further insight into enzyme for glucose monitoring applications see [7]). The Sensor Probe is a round platinum electrode with a multi-layered membrane technology. The reaction allows glucose to be converted into an electronic signal [2], which is sent wirelessly via radio frequency (RF) to the Receiver by the Transmitter, with an average lag time of 5 minutes. The Receiver converts the signal to a glucose reading that is displayed to the user.

1.5 Aim of the Work and Outline

In the previous Sections we have discussed capabilities and drawbacks of CGM devices. The aim of this work is to classify, analyze and model three of the most common transient failures we have found in CGM readings we were provided, in order to eventually simulate them.

Chapter 2 consists of the description of the two data sets we were provided and on which we led our investigation.

Chapter 3 is dedicated to the first kind of fault we have found and analyzed, and we called it *disconnection*. This failure is due to the loss of at least one sample from CGM readings for technological reasons. The collected set of disconnections was statistically investigated, and a model was proposed and validated.

Chapter 4 illustrates the second kind of fault we have found, and we called it *invaid output*. This failure can be read as an 'error code' of the CGM signal, since the receiver displays a glycemic level of 9 or 10 mg/dl. Along with a statistical investigation of the invalid outputs we have detected, a model was proposed and demonstrated to be acceptable for *short-lasting* invalid outputs.

Chapter 5 is the core of this work, and shows the most interesting results. The subject of this Chapter is the analysis of a third kind of failure, that we have called *loss of sensitivity* of the

CGM signal. This fault is not well-rendered like the other two, so it is important to detect it and model it. Losses of sensitivity are due to a transitional pressure applied to the sensor that acts as a low pass filter. Hence, a good model for this kind of failure is to consider it as a disturb consisting of a step function filtered by a first order system. The model we have proposed was eventually validated.

Chapter 6 shows the simulated transient failures with the previously discussed models, with an application on simulated CGM profiles.

2

Features of the two datasets

In this chapter we will describe the two datasets available for modeling CGM faults. Both the datasets were obtained with Dexcom® SEVEN® PLUS CGM sensors discussed in chapter 1, in two different trials overall. We were provided with 94 CGM signals on the whole, each of them lasting 7 days on average. For some shorter period frequent BG samples were also available, and this information can be exploited to classify faulty measurements.

2.1 First dataset

The first dataset we have taken into account is collected by the Artificial Pancreas (AP) at home consortium. AP@home is an European research project funded by the European commission; its aim is to improve treatment of patients with diabetes at home by enhancing closed-loop algorithms for artificial pancreas (AP) system that can be used in daily practice. For a description of the basic strategy that the European consortium AP@home plans to follow in its attempt to develop an artificial pancreas system see [6, 25].

2.1.1 Study design

The study is a multinational open-label trial involving four Clinical Research Centres (CRC), reported in Table 2.1. Sensor data were collected over the course of a 7 day period most of which are in an outpatient setting; patients visited CRC on day 1 and day 7 for insertion and removal of the two Dexcom® SEVEN® PLUS CGM sensors and on day 3 for Blood Glucose (BG) measurements. Both sensors were calibrated right after the insertion, but then underwent different calibration schedules, in order to compare the built-in calibration of the sensor with the recalibration algorithms developed for the smart sensor, i.e. a CGM sensor provided with algorithms able to generate alerts when glucose concentration is predicted to exceed the normal range threshold [8].

Reference blood glucose samples were gathered during study day 3, from 7pm to 4pm of

Academic Medical Centre Amsterdam	The Netherlands, EU
Medical University Graz	Austria, EU
Profile Institute for Metabolic Research GmbH	Germany, EU
University of Padua	Italy, EU

Table 2.1 European centres involved in the study

the day after. Blood samples were drawn every 15 minutes during the day and every 2 hours during the night; all blood samples were analyzed using the blood glucose Analyzer from Yellow Spring Instruments (YSI) laboratories. This kind of information is useful to our purposes as it allows us to classify as faulty some CGM samples with a higher rate of certainty.

2.1.2 Subject demographics

This study included 12 patients with T1DM, 3 in each of the four participating clinical centres of the consortium; all of them were aged at least 18 years, treated by basal-bolus insulin therapy using Continuous Subcutaneous Insulin Infusion (CSII) for at least 3 months and trained in carbohydrate counting; lastly, Body Mass Index (BMI) lower than 35 kg/m^2 was an inclusion criterion.
Furthermore, pregnant or breast feeding patients were not admitted to the study, nor patients with a history of myocardial infarction, acute coronary sindrome, therapeutic coronary intervention and coronary bypass.

Since 2 CGM sensors were inserted in each patient and one patient had withdrawn, we could observe 22 signals from this first dataset. Figure 2.1 displays an example of the data collected in Germany (see Table 2.1).

2.2 Second dataset

The second dataset that we used is the one considered in [1]: the aim of the study was to evaluate whether continuous glucose monitor alerts are capable of both detecting and predicting low and high BG events.

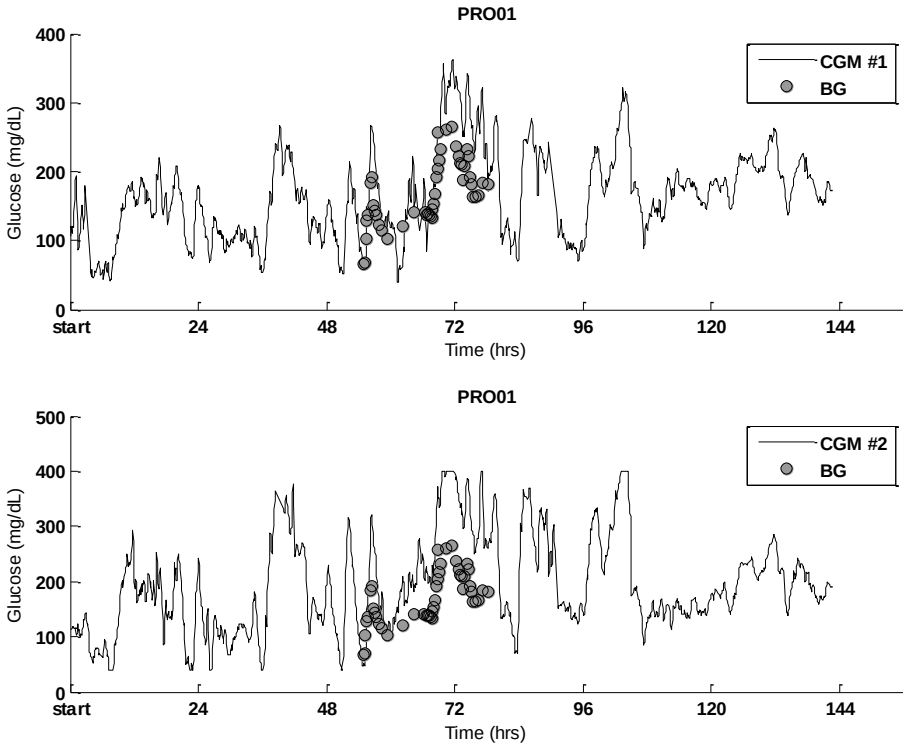

Figure 2.1 *CGM data from the 2 sensors on one patient (patient #1 in Germany). Time flowing is measured from the insertion of the sensor.*

2.2.1 Study design

Each subject wore the Dexcom® SEVEN® PLUS CGM sensor for 7 days and underwent an 8-hour in-clinic session on day 1, 4, or 7. During the in-clinic session, venous plasma samples were taken every 15 minutes with a Yellow Springs Instruments (YSI)-2300. Patients involved in the study were instructed to calibrate the sensor twice per day with a BG meter.

2.2.2 Subject demographics

CGM and reference BG data were collected from 53 adults with insulin-dependent diabetes, 81% of them affected by T1DM. These patients were gathered across three sites within the United States, and wore 72 sensors: 18 people wore 2 sensors, 35 people wore 1 sensor and 1 sensor was replaced.

The mean age of patients is 47.3 years old, with a standard deviation of 12.4; 22 subjects were female (42%), 50 were Caucasian (94%), 26 delivered insulin via multiple daily injections and their mean BMI was 27.9kg/m^2 with 7.7 as standard deviation.

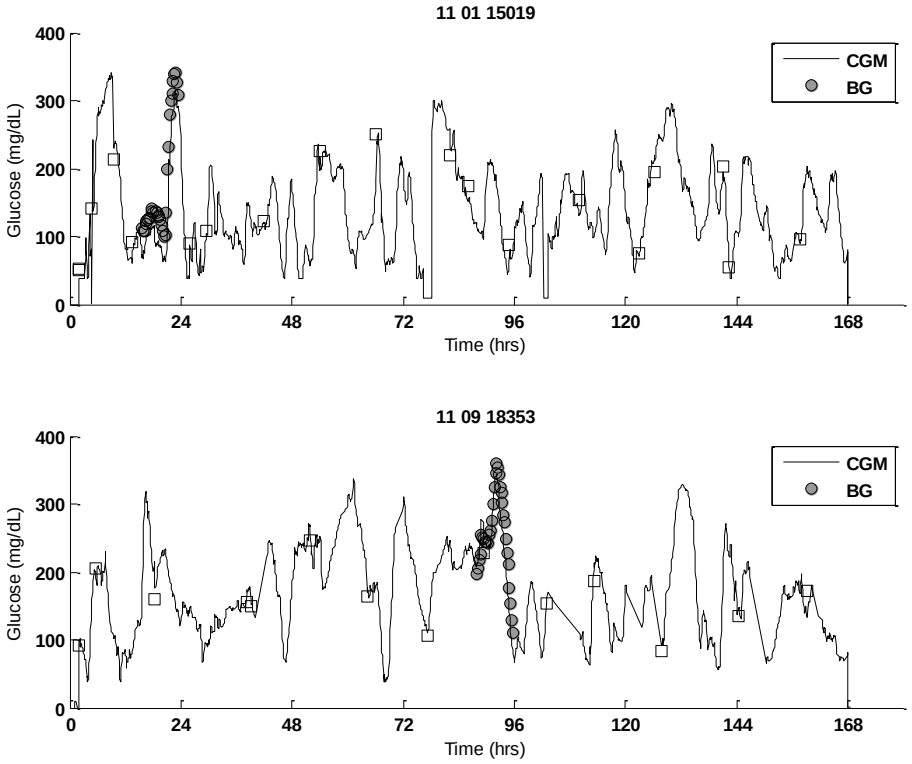

Figure 2.2 *CGM data from the sensor on two different patients. Time flowing is measured from the insertion of the sensor. The square markers reveal calibration events.*

3

Analysis of the disconnection fault

In the previous chapter the two datasets have been described. We have shown that the signals were approximately seven-days lasting data, with a sampling period of 5 minutes. BG samples were also gathered for a shorter period of time during the CGM measurement, usually for 24 hours. In fact, BG measurement requires invasive treatment that needs to be done in the hospital, where patients were admitted for short periods of time during CGM monitoring. We investigated the CGM data in order to detect any dysfunctional behaviour of the sensors with no forecast for the shapes we would find, using BG as a reference when available.
The first kind of fault is hereinafter discussed, together with its main features and stastistical parameters, gathered for simulation purposes. We will refer to it as *disconnection*. This type of error consists of the loss of at least one sample, and it is detected by investigating time occurances of the data. We found 3868 disconnections overall.

3.1 Disconnections

As discussed in Section 1.4, the SEVEN® PLUS Transimitter, mounted on the Sensor, sends the glucose readings to the Receiver every 5 minutes approximately. If we find out that the lag between two adjacent samples is significantly larger than 5 minutes, then we can state that an error had occured, as shown in Figure 3.1. We shall call *disconnection* this type of fault, since Transmitter and Receiver seem to interrupt their wireless communications for at least one sample.

We consider this type of fault mainly due to a pure technological error of the sensor or to a bad management of the sensor for a short period. This is why we chose not to include in our analysis faulty intervals larger than 75 minutes, believing that if the signal is missing for a larger interval it means that the patient has surely forgotten to keep the Receiver within the proper radius. We cannot ignore that our decision is a critical topic and should be investigated taking into account an analysis of patients' compliance.

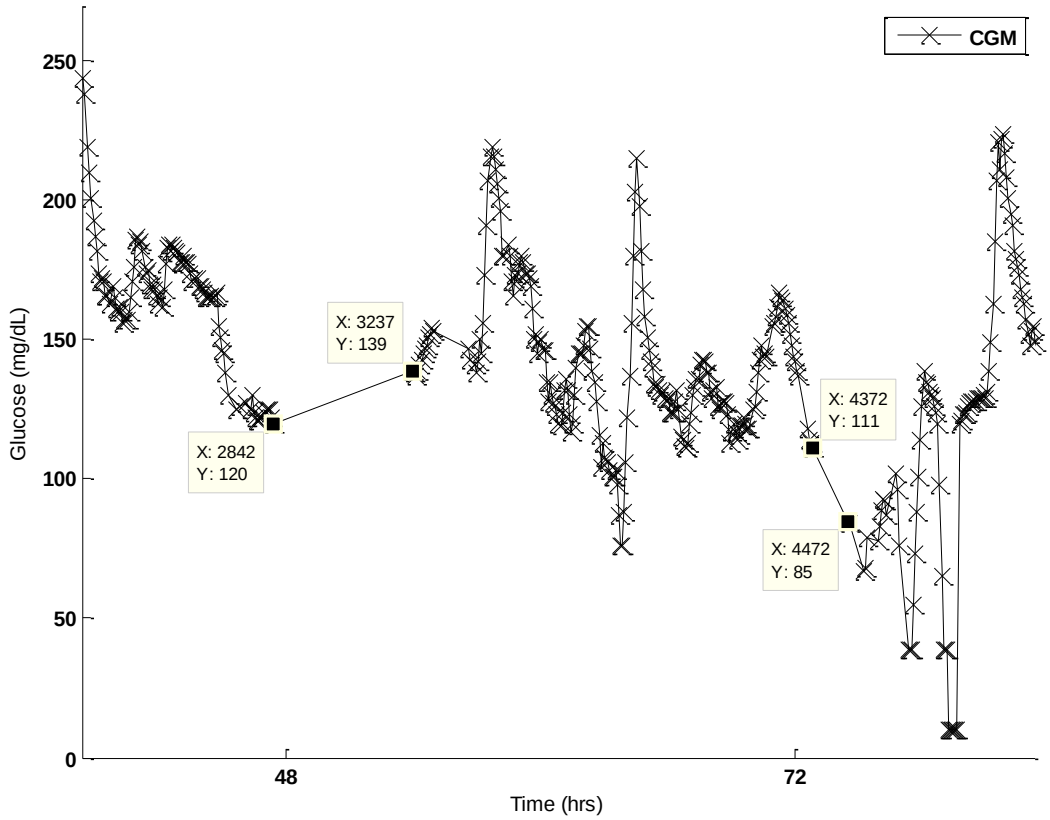

Figure 3.1 *The tips define two examples of disconnection fault. The X-coordinate displayed by the labels is measured in minutes and show the faulty distance between two samples in a row.*

All the 94 CGM signals described in Chapter 2 were considered in this first analysis. In order to detect the errors, we investigated time occurrences of the data, by verifying if the lag between one sample and the next was approximately equal to the sampling period of the sensor. If this was not true, i.e we chose a 7-minutes minimum lag, we considered the interval between the two samples as *faulty*, meaning that some data had got lost. With this isolation procedure, 3868 disconnections have been found.

For each detected fault we recorded its beginning and length, both measured in minutes from the midnight of the day of insertion of the sensor. This information was then considered in a statistical approach, as described later on in Sections 3.2, 3.5.1 and 3.5.2.

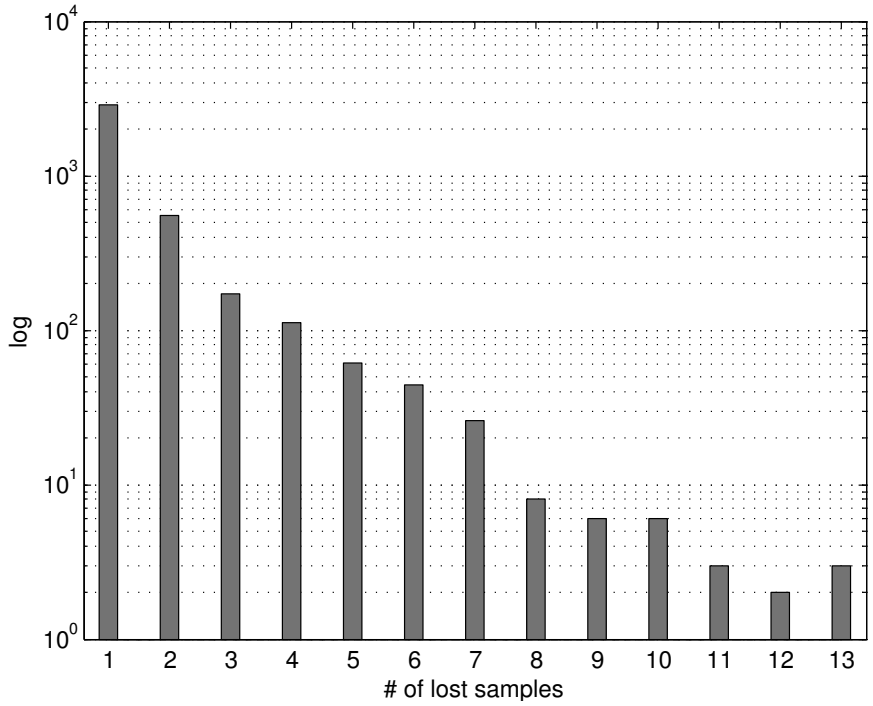

Figure 3.2 *Histogram of the number of lost samples due to disconnection error. The ordinate is logarithmically scaled.*

3.2 Duration of disconnections

As discussed in Section 3.1, we defined an upper bound to the length of the errors we were detecting, i.e. the maximum length of a disconnection is of 75 minutes. Figure 3.2 shows the histogram of the several lengths of the disconnections overall. In the abscissa we read the number of samples that are missing in the faulty interval, i.e. if we detect a 10-minutes lag between two samples in a row, that means that 1 sample had gone lost.

The highest number of disconnections consists in a loss of 1 sample (2875), and the histogram suggests that durations exponentially decrease. On average, a disconnection consists in the loss of 1.54 samples with a standard deviation of 1.2 samples (12.7055 minutes, with a standard deviation of 6.4075 minutes), while mode and median coincide at 1 sample (10 minutes).

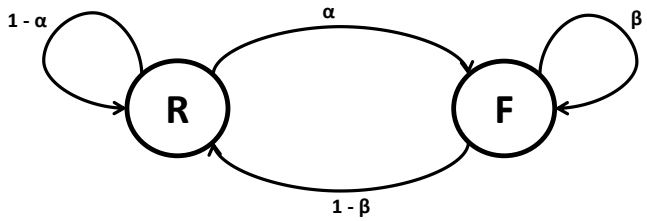

Figure 3.3 *Two-state Markov model for disconnections.*

3.3 Data modeling

In this Section we propose a reasonable model for the CGM signal with which we can explain the disconnection fault and we will show in Section 3.4 that our idea justified. CGM sensor functioning can be modelled with a two-state Markov chain. A Markov chain is a mathematical system that undergoes transitions from one state to another according to certain probabilities (called *transition* probabilities), between a finite or countable number of possible states. The "system" is a random process characterized as memoryless: the next state depends only on the current state and not on the sequence of events that preceded it. This specific kind of memorylessness is called Markov property.

Figure 3.3 shows the two-state Markov chain we consider in order to explain the transition from the regularly working state (R) to a faulty state (F). Every regular sample is followed by a faulty one with probability α, or by a regular one with probability $1 - \alpha$, while every faulty sample is followed by another faulty sample with probability β, or by a regular sample with probability $1 - \beta$.

3.3.1 Estimate of α

The transition probability α corresponds to the probability of a faulty sample to succeed a regular one. i.e. it allows us to compute when a failure occurs. It is estimated as follows:

$$\hat{\alpha} = \frac{\text{\# detected faults}}{\text{\# samples observed overall - \#faulty samples}}. \tag{3.1}$$

The estimated value is $\hat{\alpha} = 0.0230$.

3.3.2 Estimate of β

The transition probability β corresponds to the probability of a faulty sample to succeed another faulty sample, i.e. it allows us to compute the duration of the failure once it has already started.

Given that N is the number of possible durations we found in the statistical analisys 3.2, we can compute $N-1$ probabilities that a disconnection that lasted i samples, lasts $i+1$ samples. We shall define this probability as:

$$\hat{\beta}_i = \frac{\#[d \geq i+1]}{\#[d \geq i]}, \qquad i = 1, \ldots, N-1. \tag{3.2}$$

Assuming that the probability to remain in the faulty state does not depend on the duration of a disconnection, we can evaluate an average value for the transition probability β as follows:

$$\hat{\beta} = \frac{1}{N} \sum_{i=1}^{N} \hat{\beta}_i. \tag{3.3}$$

The estimated value is $\hat{\beta} = 0.5665$.

Nevertheless, we can choose to rely mostly in shorter disconnections, where the sample is larger, and compute the value for the transition probability β e.g. averaging only the first three values of the $\{\hat{\beta}_i\}$ set, or the first seven values of the $\{\hat{\beta}_i\}$ set:

$$\hat{\beta}_3 = \frac{1}{3} \sum_{i=1}^{3} \hat{\beta}_i, \qquad \hat{\beta}_7 = \frac{1}{7} \sum_{i=1}^{7} \hat{\beta}_i. \tag{3.4}$$

We will show in Section 3.4 which one of the three proposed values for β is the most appropriate, but we have to point out that some other options are also available and not taken into account in this work: for example, averaging among the $\{\hat{\beta}_i\}$ can be done with a matrix that weights the values differently according to their reliability.
The estimated values for the probabilities defined in Equation 3.4 are $\hat{\beta}_3 = 0.4377$ and $\hat{\beta}_7 = 0.5126$.

3.4 Validation

Observing the Markov chain described in Section 3.3 we can state that the probability for a disconnection to last at least one sample is the transition probability α. Then, the probability for a disconnection to last at least two samples is the product of the probability to fall into the faulty state, that is α, and the probability to remain in the faulty state for the next sample, that is β. We can write this as follows:

$$P[d \geq 1] = \alpha$$

$$P[d \geq 2] = \alpha\beta$$

$$P[d \geq 3] = \alpha\beta^2$$

and by induction:

$$P[d \geq n] = \alpha\beta^{n-1}$$

Nevertheless, from the histogram discussed in Section 3.2 we can evaluate probabilities such as P[duration is equal to k samples]. Hence:

$$P[d \geq k] = P[d = k \cup d \geq k+1] = P[d = k] + P[d \geq k+1]$$

$$P[d = k] = P[d \geq k] - P[d \geq k+1].$$

If we introduce α and β in the notation we find:

$$P[d = 1] = P[d \geq 1] - P[d \geq 2] = \alpha - \alpha\beta = \alpha(1-\beta)$$
$$P[d = 2] = P[d \geq 2] - P[d \geq 3] = \alpha\beta - \alpha\beta^2 = \alpha\beta(1-\beta)$$
$$P[d = 3] = P[d \geq 3] - P[d \geq 4] = \alpha\beta^2 - \alpha\beta^3 = \alpha\beta^2(1-\beta)$$

and by induction:

$$P[d = k] = \alpha(1-\beta)\beta^{k-1}.$$

Therefore we obtain:

$$logP[d = k] = log\frac{\alpha(1-\beta)}{\beta} + klog\beta. \tag{3.5}$$

Equation 3.5 can be read as the equation of a line, whose slope is $log\beta$ and y-intercept is $log\frac{\alpha(1-\beta)}{\beta}$. Hence, transition probabilities α and β could be computed from the histogram in Figure 3.2 as the defining parameters of the line whose equation is 3.5.

Figure 3.4 shows the result (blue line) if we draw the line with $\hat{\alpha}$ and $\hat{\beta}$ estimated in 3.3.1 and 3.3.2. The red line and the green one correspond to the estimated parameters defined in Equation 3.4. We can observe that the three lines fit more precisely the values of the histogram for # lost samples $= 1$, where the sample is larger. The red line seem to fit more precisely overall than the other two estimated lines, so our choice is to consider $\hat{\beta}_7$ as the proper value for the transition probability β.

3.5 Revising probabilities considering the day and the hour

We wonder if failures' occurances depend on the hour of the day and on sensor day, i.e. the moment from sensor insertion. In order to answer this question, we need to investigate whether

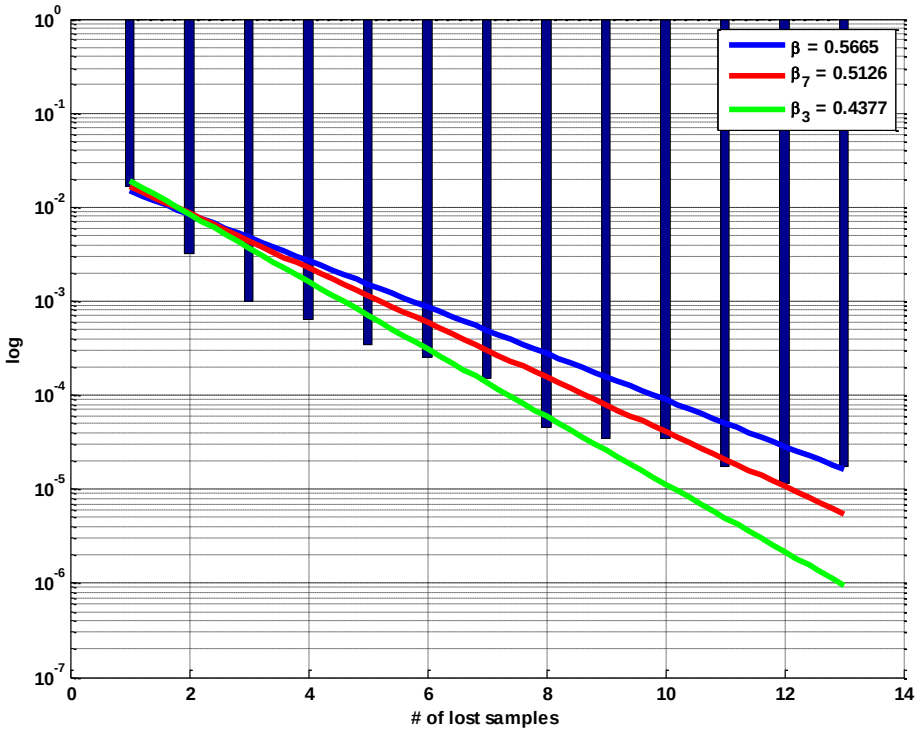

Figure 3.4 *Graphic validation of the model: the lines drawn with the estimated parameters $\hat{\alpha}$ and $\hat{\beta}$ fit the normalized histogram of disconnections' durations. In the legend are displayed the three estimated values of $\hat{\beta}$, depending on the confidence we have in the data.*

failures occur evenly both during the several days and during the several hours of the day, exploiting a statistical analysis, that is hereinafter discussed.

3.5.1 Time from insertion

In order to visualize how the disconnection event occurs during the experiment, we plotted the information about the start of each fault using a histogram as shown in Figure 3.5.1. The starting points were measured from the insertion of the sensor, thus we are here analyzing sensor's behaviour during sensor life. During our investigation we did not consider those pieces of CGM signal which were recorded after the end of the 7-th day of trial: in fact, even though the approval of the SEVEN PLUS sensor is for up to 7 days of monitoring, some monitoring session ended late.

During *day-5* we observe the highest number of errors (693), and they are distributed over the several days of trial with a mean value of 483.5 disconnections per day, standard deviation

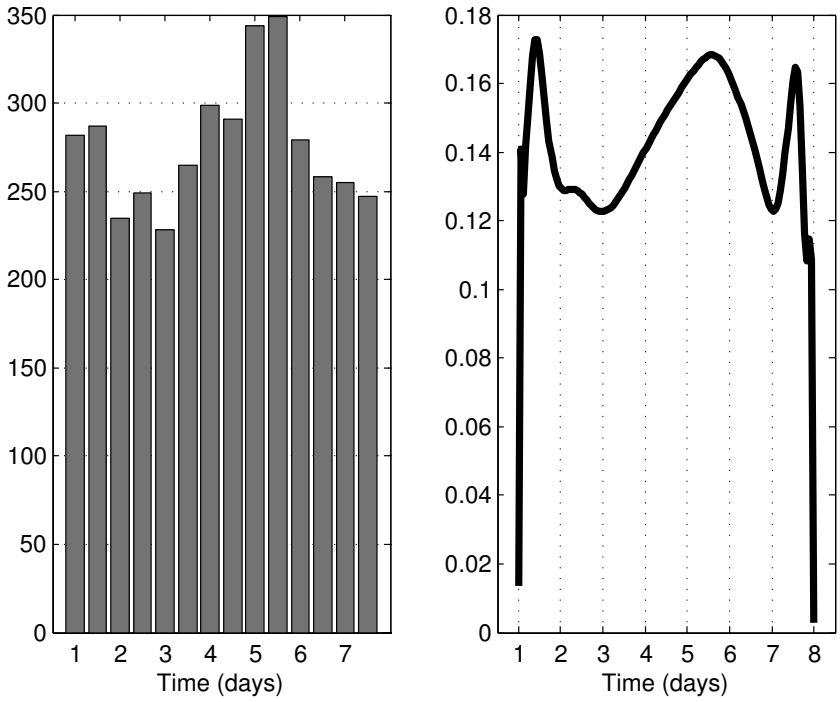

Figure 3.5 *Distribution of disconnections over the several trial days, with failures' starting points measured from the insertion of the sensor. Left panel: histogram, each day involves* 2 *bins of* 12 *hours,* Mean: 3.5242, stdev: 1.9744, median: 3.5979. *Right panel: probability density function obtained via kenel density estimation.*

of 206.9 and median of 519.5. On *day-1* we found 569 disconnections, and this is probably due to the inaccuracy of the sensor at the beginning of its monitoring session. During *day-4* and *day-5* we recorded the two highest amounts of errors: we can assume that in this phase of the trial the patient might have relaxed his careful behaviour in the management of the sensor.

The right panel of Figure 3.5.1 shows the probability density function obtained with kernel density estimation approach, described in Appendix A. The estimation was done at 120 equally spaced points, with a bandwidth of the smoothing window of 0.3074.

3.5.2 Distribution over 24 hours

In Section 3.5.1 we have investigated the time occurances of disconnections with respect to sensor life. Now we want to understand how disconnections occur during 24hours-periods. Firstly, we considered every single day of the trial as a case study. The results, displayed in Figure 3.5.2, show the probability density function, obtained via kernel density estimation (see

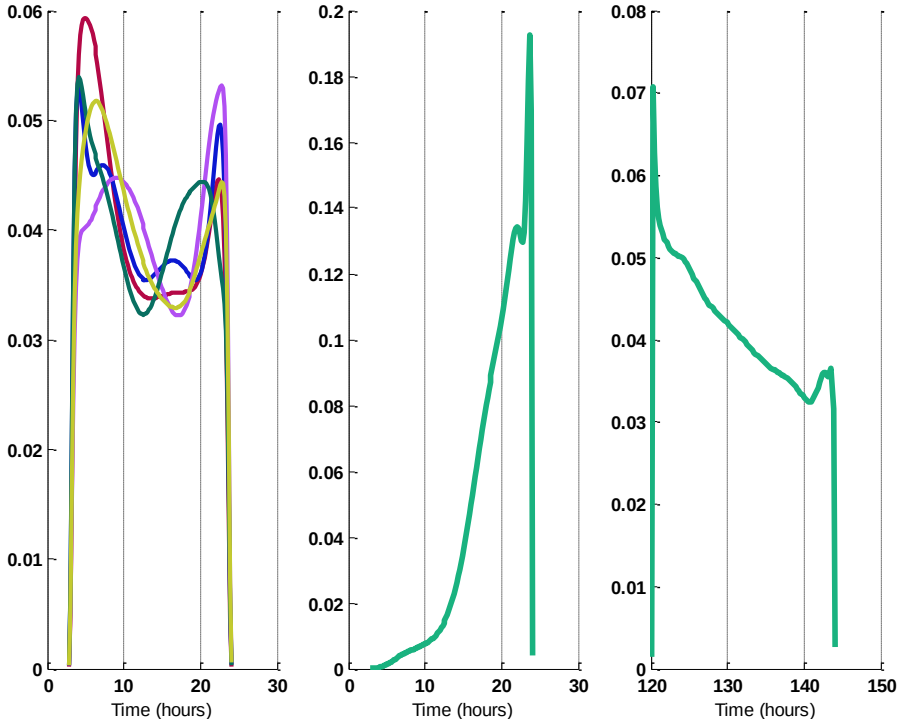

Figure 3.6 *Left panel: probability density functions for disconnections occurrences during days* #2, #3, #4, #5 *and* #7. *Middle panel and right panel: probability density functions for disconnections occurrences during days* #1 *and* #6. *The estimation is obtained via kernel density estimation approach*.4

Appendix A), of disconnections during the several days. The left panel of the Figure shows five estimated probability density functions overlapped, corresponding to days #2, #3, #4, #5 and #7. We can see that these five curves are quite similar, while middle and right panel separately show the ones corresponding to days #1 and #6. The curve in the middle panel is spoiled by the fact that the time of sensor insertion is different for every trial, while the curve in the right panel is biased because many trials ended by the afternoon of the sixth day. For these reasons, we are showing them separately, and we can conclude that for the other days there is no significant variability between one day and the other. Hence, we chose to analyze an average value of the distribution, obtained considering all days to be equivalent.

Considering every disconnection as if they occurred in one single day, we could observe the distribution of the errors depending on the hour of the day. As shown by the histogram in the left panel of Figure 3.5.2, the highest number of disconnections occurs at 6am (217), and they are distributed over the 24hours with a mean value of 154.7 disconnections per hour,

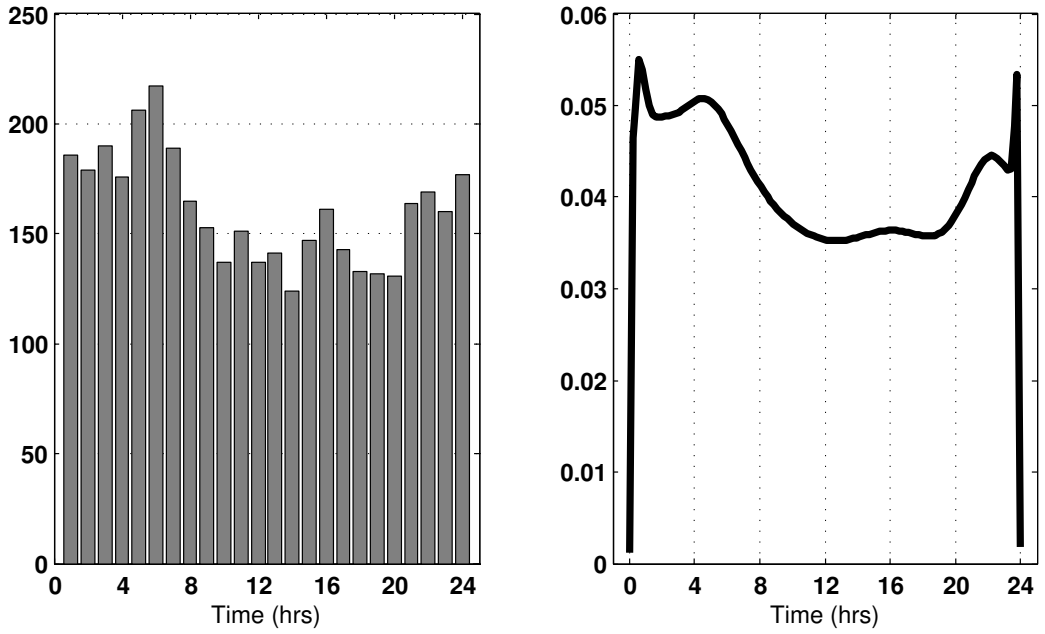

Figure 3.7 *Distribution of disconnections over 24 hours. Left panel: histogram;* mean: 11.4629, st dev: 7.1441, median: 10.8504. *Right panel: probability density function estimated via kernel density estimation approach.*

standard deviation of 40.5 and median of 154.7. The histogram shows that the highest number of disconnection occur during night-time (from 9pm to 8am). In this phase of the day, the patient is more likely to be in the sorroundings of the receiver, so we can assume that disconnections are probably mainly due to a technological failure of the sensor, rather than improper management of the device.

In the right panel of Figure 3.5.2 is the probability density function obtained with kernel density estimation approach (see Appendix A). The estimation was done at 120 equally spaced points, with a bandwidth of the kernel smoothing window of 0.3489.

3.5.3 Revising transition probability α

According to Sections 3.5.1 and 3.5.2, failures do not occur evenly neither during the several days nor during the several hours of the day. This remark suggest we should take into account revising the transition probability α described in Section 3.3.1. The transition probability from the regular-state to the faulty-state should depend also on the hour and the day of the week of the current state.

Hence, we look for the probability of a failure event, given the fact that the current day is *day*, that is, with the use of Bayes' rule:

$$P[f|\text{DAY = day}] = \frac{P[f \cap \text{DAY = day}]}{P[\text{DAY = day}]} = \frac{P[\text{DAY = day}|f]P[f]}{P[\text{DAY = day}]}.$$

From the histogram discussed in Section 3.5.1 we can compute $P[DAY = day|f]$, while $P[f]$ is $\hat{\alpha}$ and $P[DAY = day]$ is equal to $1/7$. The probability we are looking for can be written as:

$$P[f|\text{DAY = day}] = 7 \cdot P[\text{DAY = day}|f] \cdot \hat{\alpha}.$$

The same argument still holds for the case of the different distribution of disconnections over the 24hours, therefore we can conclude that the transition probability α we are looking for is:

$$P[f|\text{DAY = day, HOUR = hour}] = 24 \cdot 7 \cdot P[\text{DAY = day}|f]P[\text{HOUR = hour}|f] \cdot \hat{\alpha}. \tag{3.6}$$

4

Analysis of the invalid output fault

After the analysis of a first type of error, the disconnection, we focus on a second type, and we shall call it *invalid output*. The invalid output can be read as an 'error code' of the CGM signal, since the receiver displays a glycemic level of 9 or 10 mg/dl.
We recorded time occurances of the errors, in order to analyze its main statistical parameters for simulation purposes. Our investigation led us to find 173 invalid output overall, and we discovered that only the signals from the data set 2.2 were corrupted by this fault (72 CGM signals out of the 94 we were provided).

4.1 Invalid Outputs

As discussed in Section 1.4.1, the SEVEN® PLUS sensor does not display glucose values outside the range 39-400 mg/dl, and every value below 39 mg/dl corresponds to an 'error code' reporting that a problem had occurred. At first glance the readings from the two data sets (described in Chapter 2) show indeed frequent drops of the signals below the lower bound fixed by Dexcom®. The value displayed by the receiver component in these cases is 9 or 10 mg/dl, and we shall call *invalid output* this type of fault. Figure 4.1 depicts an example of CGM signal corrupted by invalid outputs.

We can speculate that this kind of error depends on the data smoothing activity of the sensor. Unfortunately, details on filtering strategy used by SEVEN® PLUS are not available to the public. Nevertheless, assuming that the sensor embeds a moving average filter (or more generically a finite impulse response filter), the residual between the current datum and the latest previous samples is evaluated. If the residual is larger than a threshold, then the datum is considered to be not reliable, and no valid datum is displayed until the residual lowers back under the threshold [11].

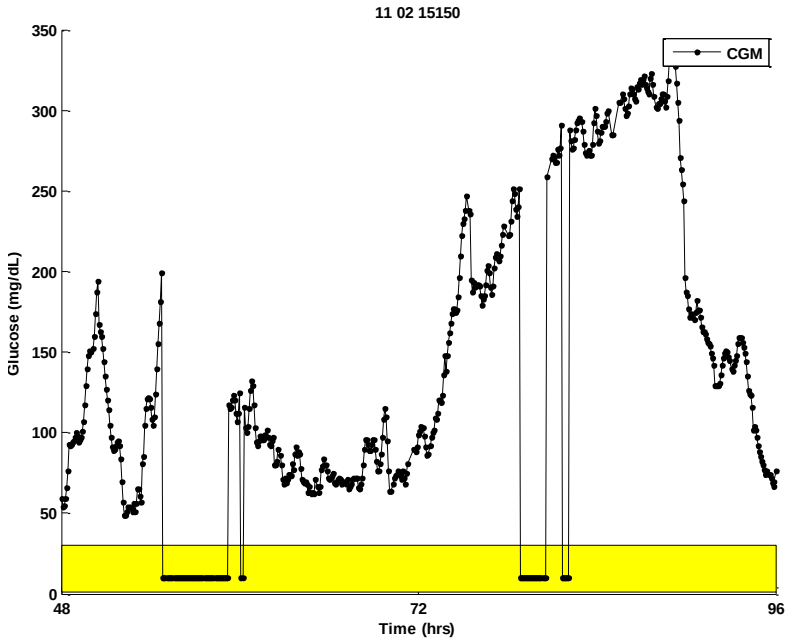

Figure 4.1 *Portion of CGM signal with invalid outputs. The yellow area highlights the four errors.*

4.2 Duration of invalid outputs

Figure 4.2 shows the histogram of the number of faulty samples due to invalid output error. The actual range of the abscissa is 2-180 samples, but since we recorded few events that involved just one case each we chose not to depict them. The highest number of invalid outputs (22) involves only 2 samples, and the histogram suggests that durations exponentially decrease.
On average, an invalid output consisits of 22 samples, i.e. 106.5202 minutes with a standard deviation of 160.6207, while mode is 2 faulty samples,i.e. 5 minutes, and median is 8 faulty samples, i.e. 40 minutes.

4.3 Data modeling

In this Section we propose a reasonable model for the CGM signal with which we can explain the invalid output fault and we will show in Section 4.4 if our idea justified, just as previously done for disconnections. CGM sensor functioning can be modelled with a two-state Markov chain, and we redirect the reader to Section 3.3 for a formal definition of a Markov model. In Figure 4.3 we show the two-state Markov chain we are proposing, with α and β as defined in

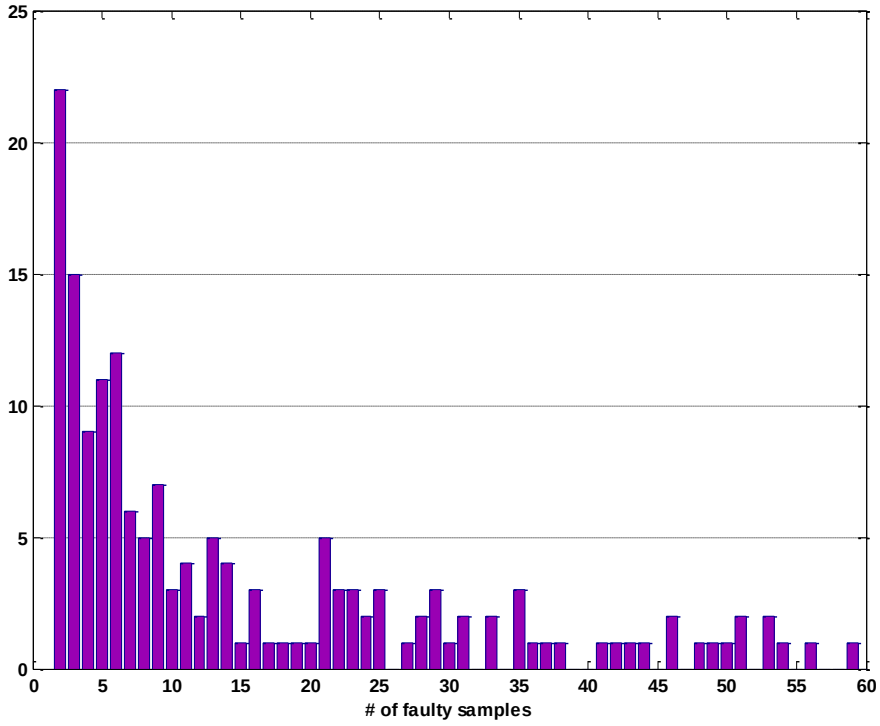

Figure 4.2 *Histogram of the number of faulty samples due to invalid output error. The Figure is focused on the most interesting interval, #1 - #60.*

Section 3.3.

4.3.1 Estimate of α

The transition probability α corresponds to the probability of a faulty sample to succeed a regular one. i.e. it allows us to compute when a failure occurs. Once again, it is estimated as follows:

$$\hat{\alpha} = \frac{\text{\# detected faults}}{\text{\# samples observed overall - \#faulty samples}}. \tag{4.1}$$

The estimated value is $\hat{\alpha} = 0.0010$.

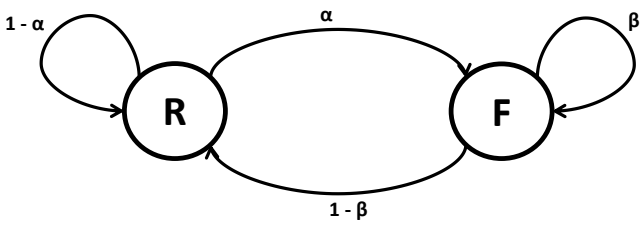

Figure 4.3 *Two-state Markov model for invalid outputs.*

4.3.2 Estimate of β

The transition probability β corresponds to the probability of a faulty sample to succeed another faulty sample, i.e. it allows us to compute the duration of the failure once it has already started. As discussed in Section 3.3.2, given that N is the number of possible durations we found in the statistical analisys 4.2, we can compute $N-1$ probabilities that a disconnection that lasted i samples, lasts $i+1$ samples. We shall define this probability as:

$$\hat{\beta}_i = \frac{\#[d \geq i+1]}{\#[d \geq i]}, \qquad i = 1, \ldots, N-1. \tag{4.2}$$

Assuming that the probability to remain in the faulty state does not depend on the duration of an invalid output, we can evaluate an average value for the transition probability β as follows:

$$\hat{\beta} = \frac{1}{N} \sum_{i=1}^{N} \hat{\beta}_i. \tag{4.3}$$

The estimated value is $\hat{\beta} = 0.9727$.

In this case as well, we can choose to rely mostly in shorter invalid outputs, where the sample is larger, and compute the value for the transition probability β e.g. averaging only the first three values of the $\{\hat{\beta}_i\}$ set, or the first seven values of the $\{\hat{\beta}_i\}$ set:

$$\hat{\beta}_3 = \frac{1}{3} \sum_{i=1}^{3} \hat{\beta}_i, \qquad \hat{\beta}_7 = \frac{1}{7} \sum_{i=1}^{7} \hat{\beta}_i. \tag{4.4}$$

We will show in Section 4.4 which one of the three proposed values for β is the most appropriate, but we have to point out that some other options are also available and not taken into account in this work: for example, averaging among the $\{\hat{\beta}_i\}$ can be done with a matrix that weighs the values differently according to their reliability.
The estimated values for the probabilities defined in Equation 4.4 are $\hat{\beta}_3 = 0.9160$ and $\hat{\beta}_7 = 0.9229$.

4.4 Validation

In order to validate the model proposed in Section 4.3, we use the same procedure discussed in Section 3.4. In Figure 4.4 we plot the three curves with equation:

$$P[d = k] = \frac{\alpha(1-\beta)}{\beta} \beta^k \tag{4.5}$$

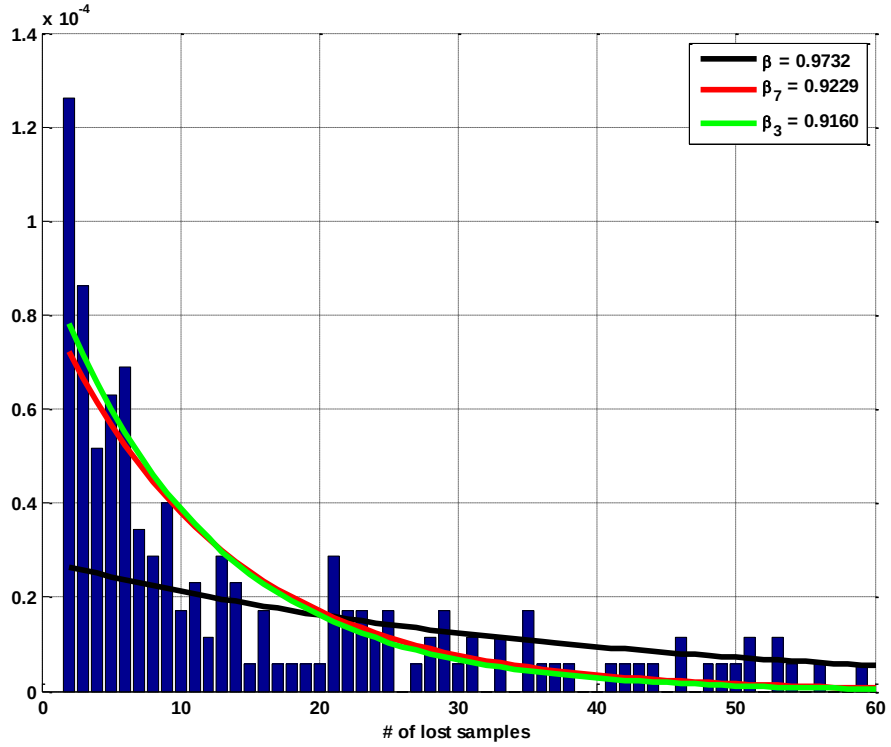

Figure 4.4 *Graphic validation of the model: the lines drawn with the estimated parameters $\hat{\alpha}$ and $\hat{\beta}$ do not fit the normalized histogram of invalid outputs' durations. In the legend are displayed the three estimated values of $\hat{\beta}$, depending on the confidence we have in the data.*

corresponding to the three different values of β estimated in Section 4.3.2.

We can point out that the fit required to the curves is not sufficient for a model validation: the black one, corresponding to $\hat{\beta}$, is biased by the several long-lasting invalid outputs (more than 60 faulty samples), while the green and the red curves yet are not a good fit of the data. Figure 4.5 shows that if we estimate $\hat{\beta}$, $\hat{\beta}_3$, $\hat{\beta}_7$ considering only short-lasting invalid outputs, i.e. failures consisting of $2 - 21$ faulty samples, the model can be considered reasonable and the curves sim to better fit the data.

Hence, we can conclude that modelling invalid outputs is an open issue, and probably the model needs to draw a distinction between short and long-lasting invalid outputs. From a simulation point of view, since we could not infer a proper model, we will draw information about invalid outputs' duration from the sampling distribution discussed in Section 4.2.

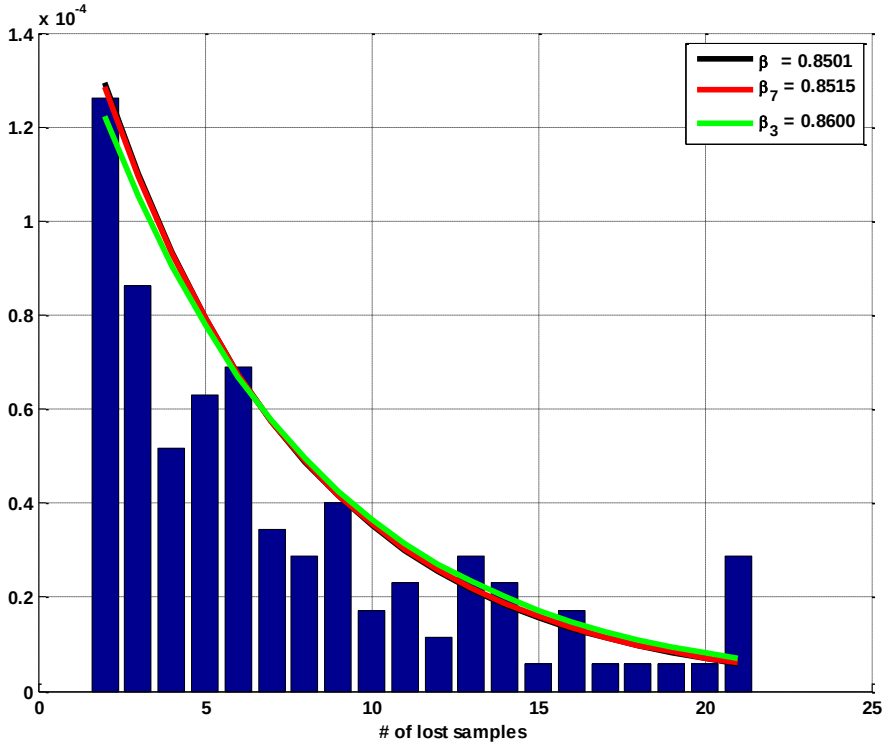

Figure 4.5 *Graphic validation of the model: the lines drawn with the estimated parameters $\hat{\alpha}$ and $\hat{\beta}$ fit the normalized histogram of invalid outputs' durations. In the legend are displayed the three estimated values of $\hat{\beta}$, estimated considering only short lasting faults ($2 - 21 samples$).*

4.5 Revising probabilities considering the day and the hour

As previously done for disconnections, we want to investigate whether invalid outputs occur evenly during the hours of the day and in the several trial days. If this is not so, we will need to revise transition probability α.

4.5.1 Distribution over the days of experiment

In order to visualize how the disconnection event occurs during the experiment, we plotted the information about the start of each fault using a histogram as shown in Figure 4.6, left panel. The highest number of invalid outputs happen during the first 24 hours of insertion (53), and the second highest amount (32) is found during the last 24 hours. This behaviour reflects that of a typical electronic device, which bad behaves at the beginning of its operative life, when defects designed into or built into a product might surface, and at the end of it, because of

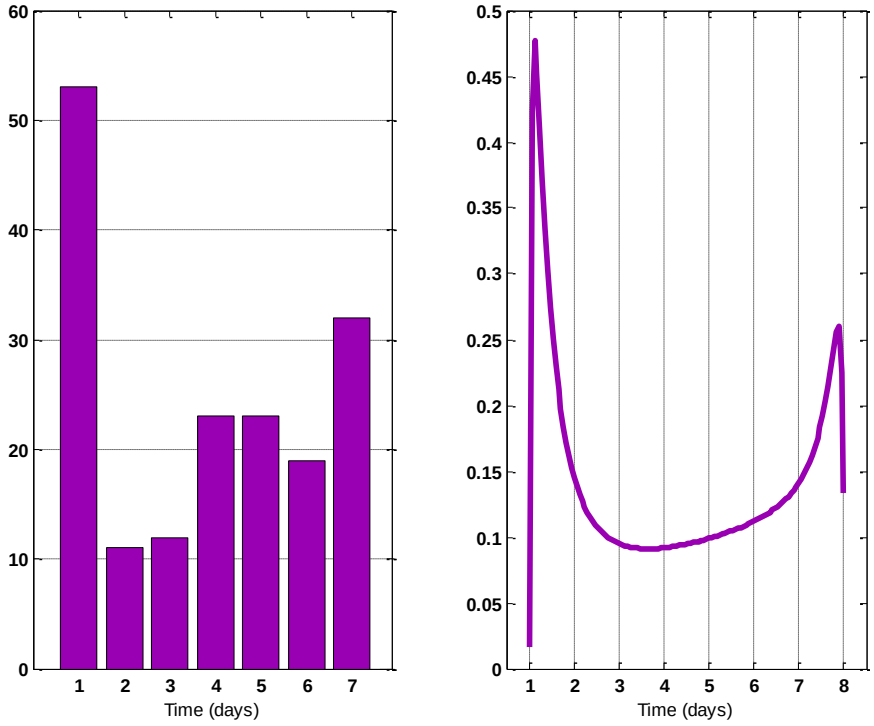

Figure 4.6 *Distribution of invalid outputs over the several trial days. Left panel: histogram;* mean: 3.2709, stdev: 2.3107, median: 3.3861. *Right panel: probability density function estimated via kernel density estimation.*

the normal wear-and-tear of components in a system. In this particular case, we also have to consider that the sensor probe needs some time to start its proper measurement because of the chemical reaction on which it is based [2].
On average, 21.63 invalid outputs occurred every day of the experiment, with a standard deviation of 15.93.

The right panel of Figure 4.6 shows the probability density function obtained with kernel density estimation approach, described in Appendix A. The estimation was done at 120 equally spaced points, with a bandwidth of the kernel smoothing window of 0.9468.

4.5.2 Distribution over 24 hours

As we have previously done in Section 3.5.2 for disconnections, we considered all the errors as if they occured in one single day. The histogram in the left panel of Figure 4.7 shows that the highest number of faults (15) occurred at 11pm, and the second highest number (14) at 8am. On

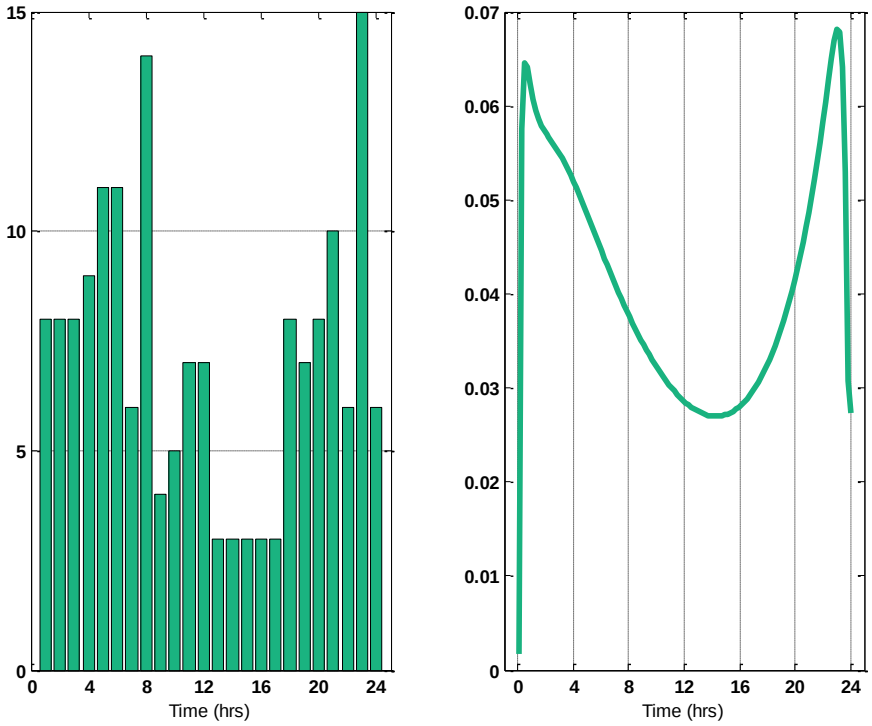

Figure 4.7 *Distribution of invalid outputs over 24 hours. Left panel: histogram;* mean: 11.6216, st dev: 7.5320, median: 10.2275. *Right panel: probability density function estimated via kernel density estimation approach.*

average, 6.92 invalid outputs are displayed every hour, with a standard deviation of 3.581 and median 7.

From the histogram we can point out that the errors occur with a higher frequency during nocturnal hours, as if they were induced by some kind of pressure while the patient is sleeping.

The right panel of Figure 4.7 shows the probability density function obtained with kernel density estimation approach, described in Appendix A. The estimation was done at 120 equally spaced points, with a bandwidth of the kernel smoothing window of 0.7414.

4.5.3 Remarks on the trend of the signal before faulty events

We have explored the 3 values of the signal before each invalid output occurred. Of these three values, mean and derivative were calculated and depicted in a scatter plot (Figure 4.8) in order to detect any possible correlation. The scatter plot shows that there is no correlation between the two values, i.e. the trend of the signal previous to the error and the average CGM value at

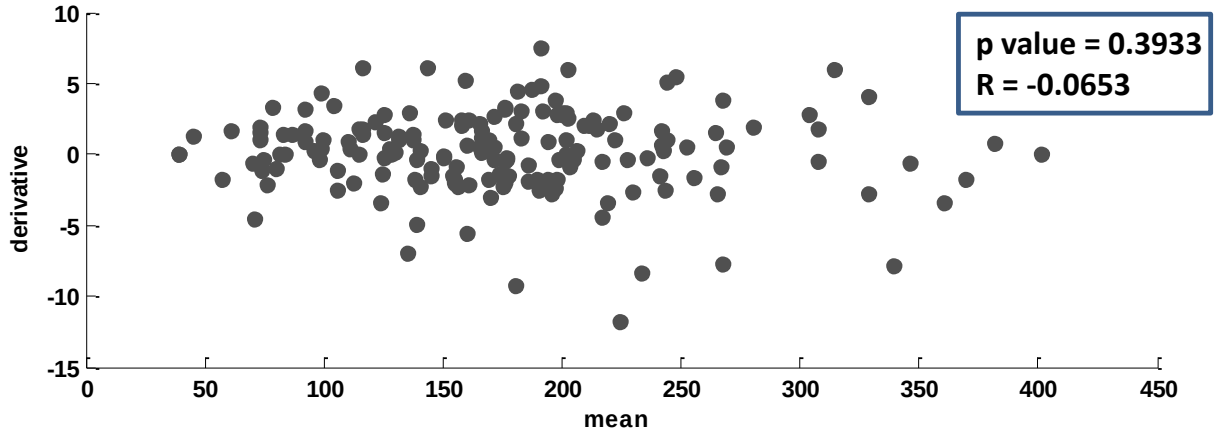

Figure 4.8 *Scatter plot of mean and derivative of the 3 samples before the error. P-values and Pearson's correlation coefficients are also displayed.*

which the error occurs are not correlated. The p-value (for testing the null hypothesis of no correlation) and the Pearson's correlation coefficient displayed in Figure 4.8 support the result. In fact, the p-value is the probability of getting a correlation as large as the observed value by random chance, when the true correlation is zero. If the p-value was small, say less than 0.05, then the correlation would be significant. In this case, the p-value is 0.3933, hence significantly larger than 0.05. Moreover, as the Pearson's correlation coefficient approaches zero there is less of a relationship (closer to uncorrelated): being $R = -0.0653$, we can state the absence of correlation.

This fact simplifies our simulation step since it allows us to consider one parameter less.

4.5.4 Revising transition probability α

As previously done in Section 3.5.3, we want to revise transition probability α, in order to describe its reliance on the hour and the day of the failure. We redirect the reader to Section 3.5.3 for the procedure, while we quote the result, that involves the estimated value $\hat{\alpha}$ from Section 4.3.1:

$$P[f|\text{DAY = day, HOUR = hour}] = 24 \cdot 7 \cdot P[\text{DAY = day}|f]P[\text{HOUR = hour}|f] \cdot \hat{\alpha}. \tag{4.6}$$

5

Analysis of the loss of sensitivity

Two types of CGM failures were discussed so far. The type of CGM failure described in this Chapter is due to biomechanics, since it arises when a pressure is applied to the sensor, and we shall call it *loss of sensitivity* of the CGM signal. Fault identification was done with visual inspection using BG as a reference when available and led us to 28 detected failures. The isolation of the faulty shapes was then done exploiting a *bayesian smoothing* of the CGM signal, and this procedure also gave us an estimation of the variance of the measurement error of the signal.
We proposed a model for losses of sensitivity, and estimated its parameters, discussing their estimation precision as well. Finally, we validated our model showing that it properly simulates the isolated shapes.

5.1 Main features

The loss of sensitivity is the third type of CGM failure we consider in this work. Its shape is shown in Figure 5.1: the error consists of a rapid decrease of the signal, followed by an increase that brings the signal back to the regular trend. This kind of fault was detected comparing the CGM signal with the reference BG samples when available, and when not, we had to observe the signal trend in the surroundings of the candidate failure in order to decide if it was so.

For what concerns the reasons that cause a loss of sensitivity, these are related more to the biomechanics of the sensor-tissue interface has been taken into account rather than to chemical biocompatibility [12]. Infact, biomechanical factors such as motion and pressure cause interfacial stresses, which affect tissue physiology around a sensor and, in turn, impact sensor performance. Motion artifacts can arise when acute forces temporarily impact sensor signal. It is hypothesized that applying direct pressure on the sensor and surrounding tissue can cause temporary reduction of localized blood flow, thus perturbing sensor readings. One common cause of acute motion artifacts is the subject lying or sleeping on the sensor: in humans, pressure at the sensor site is believed to be responsible for anomalous hypoglicemic measurements

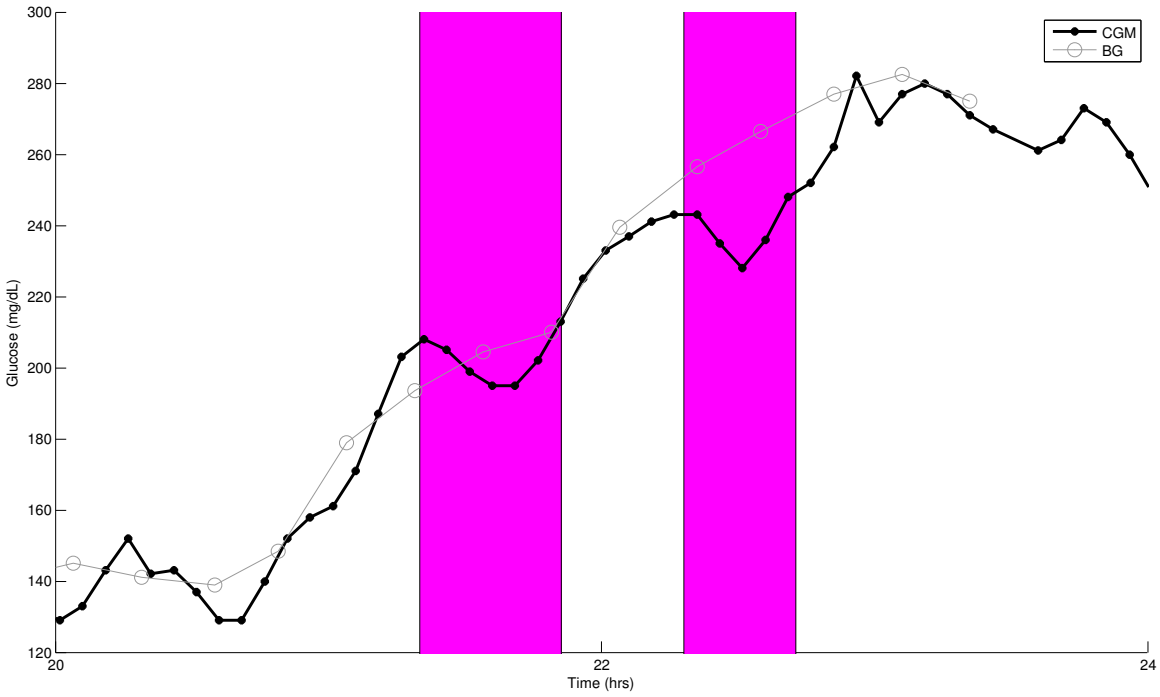

Figure 5.1 *Example of two losses of sensitivity of the CGM signal, highlighted by the pink area. Blood Glucose samples are used as a reference.*

reported at night time, particularly when the patients lie on the sensor [13].
It is relevant to report an example of the acute effects from direct pressure on the sensor, observed in a clinical trial (details in [14, 15]). CGM readings collected from patient wearing a Dexcom® SEVEN® PLUS on his abdomen show signal drops as compared to the blood glucose levels, as the patient laid on the sensor and compressed it.

5.2 Visual Identification

Unlike disconnections and invalid outputs, losses of sensitivity are not well-rendered. Hence, the identification of these types of fault was done with visual inspection, using BG as a reference when available. In order to isolate them, we followed this procedure:

1. visual identification of starting and ending point of the loss of sensitivity, exploiting BG as a reference;

2. removal of the CGM piece affected by the loss of sensitivity identificated at *step 1*;

3. interpolation of the CGM signal in the faulty interval that was cleared from the failure at *step 2*;

4. the shape of the isolated loss of sensitivity is obtained as the difference between the interpolated signal and the real CGM values in the faulty interval.

In the first place, we tried a linear interpolation of the CGM signal in the faulty interval (*step 3*). This technique demonstrated itself to be misleading, since the linear interpolation performs a rough reconstruction of the CGM signal in the faulty interval, thus spoiling the amplitude of the resulting isolated fault.

As a consequence, to improve interpolation a bayesian smoothing was applied to the CGM signal. The procedure is hereinafter discussed, in Section 5.2.1

5.2.1 Bayesian smoothing

We can start by assuming that physiological processes are smooth signals. In order to give a formal statement of the problem, we define the signal we are dealing with as

$$y = u + v \tag{5.1}$$

where y, u and v are three vectors containing a certain number of CGM measurements, real (unknown) glycemic values and measurement errors, respectively. The reconstruction of the real glycemic profile $u(t)$ starting from noisy discrete observations $y(t)$ is a classical smoothing problem, that can be treated through classical *regularization methods*. As a consequence, the first step is to introduce the problem into a *stochastic context*.

For what concerns Equation 5.1, we can assume, without loss of generality, that v and u are zero-mean random vectors with $\text{Var}[v] = \sigma^2\Sigma_v$, $\text{Var}[u] = \lambda^2\Sigma_u$, where Σ_v and Σ_u are positive define matrices, and σ^2 and λ^2 are positive scalars.

Matrices Σ_v and Σ_u express the prior knowledge of the unknown signals $v(t)$ and $u(t)$. Assuming that the measurement errors are uncorrelated and have the same variance σ^2, then the measurement noise covariance matrix can be written as $\Sigma_v = \sigma^2 I$. Furthermore, assuming the only *a priori* knowledge on $u(t)$ is that it is a regular biological signal, we can think of it as a multiple integration of a white noise process. In this way it is easily seen that its covariance matrix becomes $\Sigma_u = \lambda^2(F^T F)^{-1}$. F is a suitable design matrix:

$$F = (\Delta)^m \tag{5.2}$$

where m represents the m-order derivative penalization of the signal $u(t)$ and Δ is a Toeplitz matrix:

$$\mathbf{\Delta} = \begin{pmatrix} 1 & 0 & 0 & \dots & 0 \\ -1 & 1 & 0 & \dots & 0 \\ 0 & -1 & 1 & \dots & 0 \\ \dots & 0 & -1 & \dots & \dots \\ 0 & \dots & \dots & \dots & 1 \end{pmatrix} \tag{5.3}$$

The parameter m reflects the degree of smoothness of the signal, and our choice was $m = 2$, i.e. we evaluated the second derivative of the signal. We justify this choice referring to [9]. Using a linear mean-square estimator, given the measurement vector y, our purpose now is to find $\hat{u}$ which minimizes $E[\|u - \hat{u}\|^2]$. The regularization theory says that $\hat{u}^R$ is:

$$\hat{u}^R = \underset{\hat{u}}{\operatorname{argmin}} \left\{ (y - \hat{u})^T (y - \hat{u}) + \gamma \hat{u}^T F^T F \hat{u} \right\} \tag{5.4}$$

where the scalar $\gamma = \sigma^2/\lambda^2 > 0$ is the so-called *regularization parameter*. The first term of the cost function on the right-hand side of equation 5.4 measures the fidelity to the data while the second term weights the roughness of the estimate. The solution of equation 5.4 is:

$$\hat{u}^R = (I + \gamma F^T F)^{-1} y \tag{5.5}$$

Once m is fixed as previously described, the result is hence a function of the parameter γ. Nevertheless, in our case, both σ^2 and λ^2 are unknown.

The estimation procedure for σ^2 and λ^2 refers to *Criterion 2* discussed in [10]. When both σ^2 and λ^2 are unknown, the minimization problem of equation 5.4 should be solved for several trial values of $\gamma = \sigma^2/\lambda^2$ until:

$$\frac{WRSS(\gamma)}{n - q(\gamma)} = \gamma \frac{WESS(\gamma)}{q(\gamma)} \tag{5.6}$$

where n is the number of measurements collected in the predetermined interval considered, $WESS(\gamma)$:

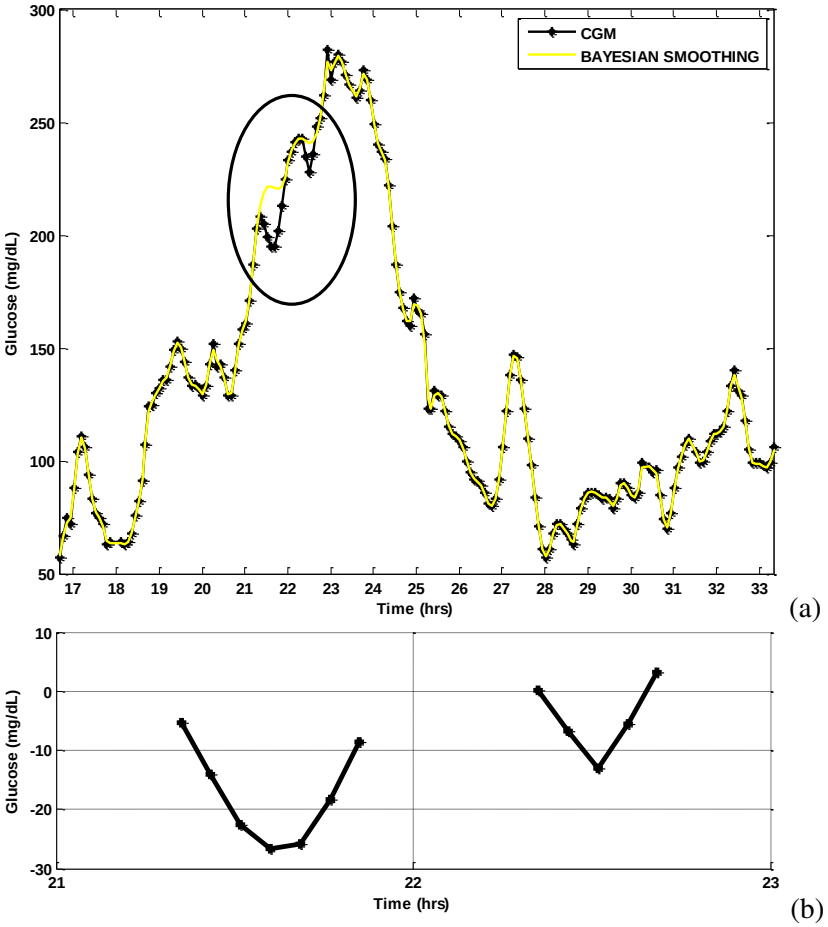

Figure 5.2 *(a) CGM signal and its bayesian smoothing, with a focus on the faulty pieces. (b) Isolated losses of sensitivity.*

$$WESS(\gamma) = \hat{u}^T F^T F \hat{u}, \tag{5.7}$$

is the weighted estimates sum of squares, $WRSS(\gamma)$:

$$WRSS(\gamma) = (y - \hat{u})^T (y - \hat{u}), \tag{5.8}$$

is the weighted residual sum of squares, and $q(\gamma)$:

$$q(\gamma) = trace[I_n + \gamma F^T F]^{-1} \tag{5.9}$$

which is termed *degree of freedom*, with I_n an n-size identity matrix.

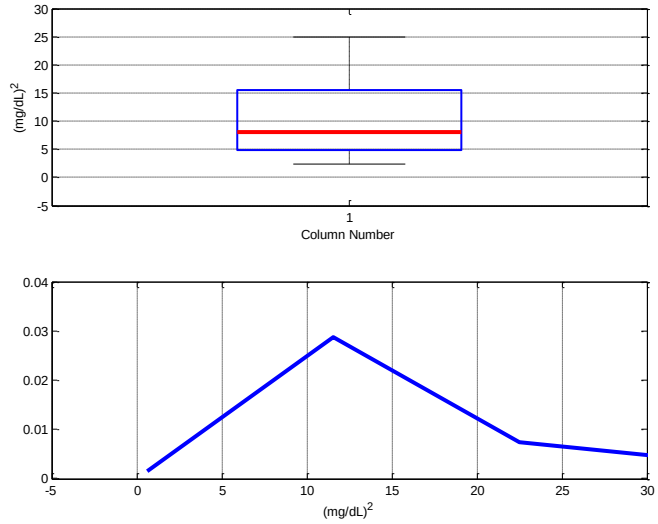

Figure 5.3 *Top panel: Boxplot of the estimated values for σ^2; red line shows the median;* mean = 8.8; st dev = 3.6; median = 8. Range of the box: 4.8-15.6. *Bottom panel: probability density function estimated via kernel density estimation*.

The so-found value of γ maximizes the likelihood of the data. As γ is determined, the estimations of σ^2 and λ^2 are given by:

$$\sigma^2 = \frac{WRSS(\gamma)}{n - q(\gamma)} \tag{5.10}$$

and

$$\lambda^2 = \sigma^2/\gamma. \tag{5.11}$$

Figure 5.2.1 shows the result of a bayesian smoothing for the CGM signal and an example of two isolated losses of sensitivity. Along with the isolation procedure, the bayesian smoothing also gave us an estimate of the variance σ^2 of the signals. With this information we can decide whether a piece of signal is faulty or noisy. We found an average value of the estimated σ^2 that is 8.8 mg^2/dl^2 with a standard deviation of 3.6 mg/dl. Therefore failures smaller than about $2SD \cong 6$ mg/dl were considered to be noise. Figure 5.3 shows the boxplot of the estimated values for σ^2.

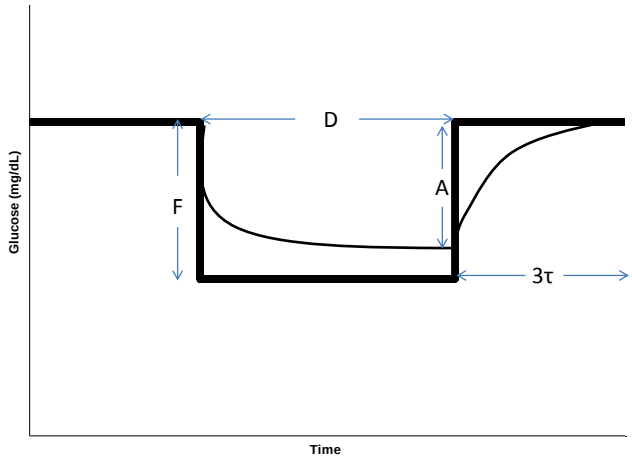

Figure 5.4 *Step function with amplitude F and duration D, that is filtered by a first order system with parameter τ. The overlapped curve shows the result of the filtered signal, with amplitude A. The time requested by this curve to reach zero is 3τ.*

5.3 Data modeling

The model for losses of sensitivity here proposed is based on biomechanical considerations drawn in Section 5.1, i.e. the failure is due to a transitional pressure applied to the sensor that acts as a low pass filter. Hence, a good model for this kind of failure is to consider it as a disturb consisting of a step function filtered by a first order system with transfer function $G(s) = \frac{1}{1+\tau s}$. The τ parameter has to be estimated together with the two defining parameters of the disturb, which are graphically described in Figure 5.3. The step function is characterized by its amplitude, and we shall call this parameter F, and by its duration D. In the same Figure we show the shape of a modelled loss, in order to describe the impact of the τ parameter. We define τ as one third of the time needed by the failure to go from its maximum amplitude (A), back to zero. The real amplitude A reached by the failure is connected to the amplitude F of the step function by the relation $F = \frac{A}{1-e^{-\frac{D}{\tau}}}$.

The equation of the model is:

$$M(p,t) = -F(1 - e^{\frac{-(t+t_0)}{\tau}})1(t+t_0) + F(1 - e^{\frac{-(t-t_0-D)}{\tau}})1(t+t_0+D) \tag{5.12}$$

with $p = [FD\tau]$. We assumed that the parameters we want to estimate do not depend on the hour of the day, and are mutually indipendent. Our model is non-linear in parameters as shown by Equation 5.12, hence we solved a non linear least squares problem for each detected and

isolated fault, in order to find the value:

$$\hat{p}_{LS} = \underset{\hat{p}}{\text{argmin}} \|z - M(p)\|^2 \tag{5.13}$$

with z being the faulty isolated CGM profile. Non-linear estimation techniques were used, such as the iterative method of Gauss-Newton. The algorithm starts with an initial guess for the minumum, p_0, and the method proceeds by the iterations
repeat

- linearization of the model with respect of the parameters of the model, in the surroundings of p_{i-1}
- solution of the linear least-squares problem gives $\Delta\hat{p}_i$
- the latest estimated $\hat{p}_i = \hat{p}_{i-1} + \Delta\hat{p}_i$

until
$|\Delta\hat{p}_i/\hat{p}_i| < tol$, with i iteration index and tol a fixed tolerance threshold.

The estimation can be biased by the initial guess, since the iterative procedure might fall into a local, rather than absolute, minumum of the function. The starting vector $p_0 = [F_0 \quad D_0 \quad \tau_0]$ for the algorithm was chosen as the average values of the same parameters evaluated for the isolated losses.

5.3.1 Precision and Statistics of the estimated parameters

The solution of the non-linear least squares problem we have previously discussed, gives us the Jacobian matrix J of the minimized function at the estimated vector $\hat{p}$. In this case, we can define the covariance matrix Σ_p in order to measure the estimation error:

$$\Sigma_p \cong (J^T \Sigma_v^{-1} J)^{-1}. \tag{5.14}$$

In our case, to each patient whose CGM signal is affected by losses of sensitivity corresponds one matrix Σ_v^{-1} defined as

$$\mathbf{\Sigma_v^{-1}} = \begin{pmatrix} 1/\sigma^2 & 0 & 0 & \dots & 0 \\ 0 & 1/\sigma^2 & 0 & \dots & \vdots \\ \vdots & 0 & \ddots & \dots & \vdots \\ \vdots & 0 & 0 & \ddots & \vdots \\ 0 & \dots & \dots & \dots & 1/\sigma^2 \end{pmatrix} \tag{5.15}$$

with σ^2 estimated along with the bayesian smoothing as discussed in Section 5.2.1. Hence, for each one of the detected and isolated fault, we can compute the estimation precision of the parameters using equation 5.14. Table 5.3.2 shows this result, highlighting those parameters whose estimation precision is bad, while Table 5.3.2 shows five interesting parameters that describe the goodness of fit for each simulated loss of sensitivity.

For what concerns failures 3, 4 and 10 shown in Figure 5.3.2, we can see that the the yellow area of $\pm 2 \cdot$ confidence interval is large and the amplitudes of the isolated shapes are small. Hence, a simpler model as well would predict a proper shape, while here we obtain bad results for FIT parameters. Moreover, the isolated shapes are less similar to the expected one shown in Figure 5.3, hence the empirical evaluation of F_0, D_0 and τ_0 is less significant and gives bad estimation precisions. We show in Figure 5.3.2 the original CGM signal where we isolated the three failures we are discussing, in order to demonstrate that our visual detection was right, but something spoiled the result during the isolation procedure.

Figure 5.3.2 shows other failures that are worth a further insight. Loss of sensitivity 12 is simulated by the model with bad values for both MSE and FIT, even though the estimation precision of the parameters of the model is good. The MSE is very high in this case because our model simulates failures starting from a zero glycemic level, while the isolation procedure does not always assure this. Also failure 22 is simulated with a bad FIT and good estimation precision of the parameters, because its shape is irregular and hard for the model to follow. Failure 16 instead is made of only 3 samples, hence the estimation of the 3 parameters of the model on such little data is understandably hard, giving bad estimation precision and yet very good FIT. Failure 24 has a very irregular shape that is hard for our model to follow, and lastly failure 25 behaves in the opposite way of what we expect, since we have described the loss of sensitivity as a *rapid* decrease of the signal (5.1).

We consider the other estimation precisions to be reasonably good.

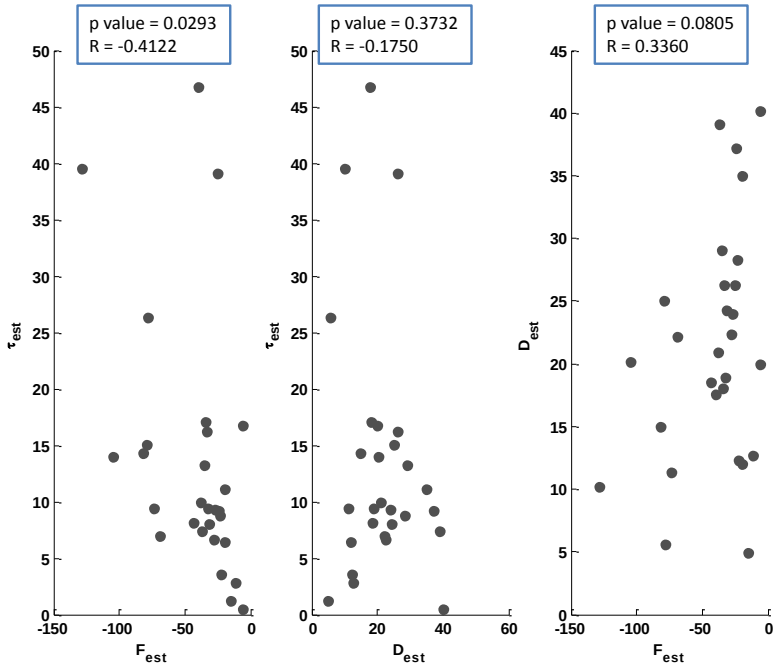

Figure 5.5 *Scatter plot of the estimated parameters (F, τ), (D, τ), (F, D). P-values and Pearson's correlation coefficients are also displayed.*

Figure 5.8 shows the histogram and the density function obtained via kernel density estimation for both initial parameters $p_0 = [F_0 \quad D_0 \quad \tau_0]$ and the estimated ones $\hat{p} = [F \quad D \quad \tau]$. We found that the estimated parameter D, i.e. the time needed to reach the maximum amplitude A, is on average 21.3 minutes, while the estimated amplitude of the step function F is on average -41.8 mg/dl. The system parameter τ is on average 13.5 minutes.

We also tried to run the estimation algorithm with the same common initial guess p_0 for all faults. The vector p_0 was chosen as the average of the empirical evaluated parameters F, D and τ on each isolated fault, as described in Figure 5.3. The statistics results for the estimated parameters is shown in Figure 5.9, in comparison to the previous estimation results displayed in Figure 5.8. This result demonstrates that our estimation method is robust to the initial guess.

5.3.2 Correlation between F, D and τ

In Section 5.3 we made two assumption. The first deals with the relationship between the failure and the moment of its occurrence: this issue will be explored in Section 5.5. The second is about the statistical relationship between the three parameters D, F, τ. We investigated this issue

with a scatter plot for each of the couples (F, τ), (D, τ), (F, D) and evaluating the p-value, for testing the null hypothesis of no correlation, and the Pearson's correlation coefficient R (we refer the reader to Section 4.5.3 for the meaning of p-value and R). Figure 5.5 shows this result.

For what concerns the couples (D, τ) and (F, D), in both cases the p-value is larger than 0.05 hence we can support the null hypothesis of no correlation. For couple (F, τ) instead, the p-value is lower than the threshold of 0.05, but $|R| < 0.5$, hence we can say that these two parameters are partially correlated.

5.4 Validation

A first validation of the model we have previously described is given in Figure 5.4. We show here with two examples that simulating the loss of sensitivity with this model leads us to a signal that is similar to the isolated real failure, and is inside the area of $\pm 2 \cdot$ confidence interval, which is obtained with the previously estimated σ^2, as discussed in Section 5.2.1. The other simulated losses of sensitivity are shown in Appendix B.

Furthermore, we chose pieces of CGM signal in which we had found no failure, and removed them as described in Section 5.2. The whole signal then underwent bayesian smoothing, and we expected the reconstructed signal to lie within the $\pm 3 \cdot$ confidence interval obtained with the estimated σ^2. Figure 5.4 shows four examples of the smoothed signal lying within the $\pm 3 \cdot$ confidence interval , which proves that isolating pieces of regular signal is not misleading.

5.5 Reliance on the hour and the day of experiment

As previously done for disconnections and invalid outputs, we wonder if transition probability $\hat{\alpha}$ should be revised considering the hour and the day at which failure occurs. Figure 5.12 shows the result for the distribution of losses of sensitivity over 24 hours and through the several days of experiment. Considering that we found a small amount of pressure faults (28), we are not revising the transition probability because we cannot gather significant information from such a

# loss	MSE	FIT (%)	COD (%)	VAPNIK	VAPNIK FIT (%)
1	4.4489	72.8399	92.6233	0.2583	93.2634
2	5.3979	58.6935	82.9377	0.11576	94.4345
3	20.0696	14.9614	27.6844	0	$\frac{0}{0}$
4	2.8256	59.3382	83.4662	0	$\frac{0}{0}$
5	17.2726	74.1279	93.3063	0	100
6	4.436	85.7085	97.9575	0	100
7	35.0123	60.8489	84.6719	0	$\frac{0}{0}$
8	35.5277	77.8835	95.1086	0	100
9	35.7024	68.6243	90.1557	0.54073	93.6721
10	24.0505	42.1049	66.4815	0	100
11	8.2897	77.0703	94.7423	0	100
12	20.036	29.5094	50.3107	0.69486	35.9385
13	6.9514	63.7941	86.8913	0.19665	94.9374
14	41.4536	41.8388	66.1728	1.5071	69.8901
15	13.2339	65.0399	87.7779	0.0042032	99.9129
16	0.2031	93.3686	99.5602	0	100
17	11.651	67.5585	89.4755	0.16306	96.6248
18	7.1542	70.5571	91.3312	0.14547	96.1511
19	4.9779	71.6762	91.9776	0	100
20	7.5477	72.7415	92.5697	0.13071	97.3613
21	20.5042	77.0219	94.7201	1.2697	90.5562
22	29.8898	32.6935	54.6983	0.57873	63.1904
23	0.67519	84.621	97.6349	0	$\frac{0}{0}$
24	11.348	39.0962	62.9073	0.50938	62.1821
25	41.7089	16.6987	30.6089	1.6655	34.6656
26	6.2978	71.049	91.6184	0	100
27	6.234	77.4247	94.9035	0	100
28	31.6266	75.6968	94.0935	1.4953	90.3779

Table 5.1 *Interesting parameters describing the goodness of our model.*

# loss	F (mg/dl), (%)	D (min), (%)	τ (min), (%)
1	-28.3, 7	22.3, 5	6.6, 18
2	-11.2, 20	12.7, 19	2.8, 73
3	-6, 646	20, 337	16.7, 1036
4	-78.4, 168	5.6, 95	26.3, 171
5	-73.5, 14	11.3, 10	9.4, 20
6	-36.6, 7	39.1, 3	7.4, 22
7	-38.4, 70	20.9, 54	10, 142
8	-104.3, 35	20.2, 25	14, 54
9	-68.8, 7	22.2, 6	6.9, 19
10	-40, 329	17.6, 77	46.8, 377
11	-43.8, 11	18.5, 6	8.2, 21
12	-22.5, 22	12.3, 20	3.6, 64
13	-34.1, 11	18, 6	17.1, 13
14	-20, 11	35, 9	11.1, 27
15	-27.5, 12	24, 6	9.3, 23
16	-14.9, 10^9	4.9, 10^9	1.2, 10^9
17	-35, 9	29.1, 5	13.2, 15
18	-246, 6	37.2, 4	9.2, 17
19	-23.7, 12	28.2, 6	8.8, 25
20	-33.6, 13	26.3, 8	16.2, 23
21	-82.2, 12	15, 13	14.3, 15
22	-128.3, 20	10.2, 13	39.5, 19
23	-19.7, 54	12.1, 38	6.4, 100
24	-25.2, 115	26.3, 27	39.1, 149
25	-5.7, 18	40.1, 10^{11}	0.5, 10^{11}
26	-32.6, 15	18.9, 8	9.4, 25
27	-31.3, 11	24.2, 5	8, 22
28	-79.3, 8	25, 5	15, 14

Table 5.2 *Estimated parameters F, D, τ described in Section 5.3 and their estimation precision. The grey shadow highlights those parameters whose estimation precision is bad.*

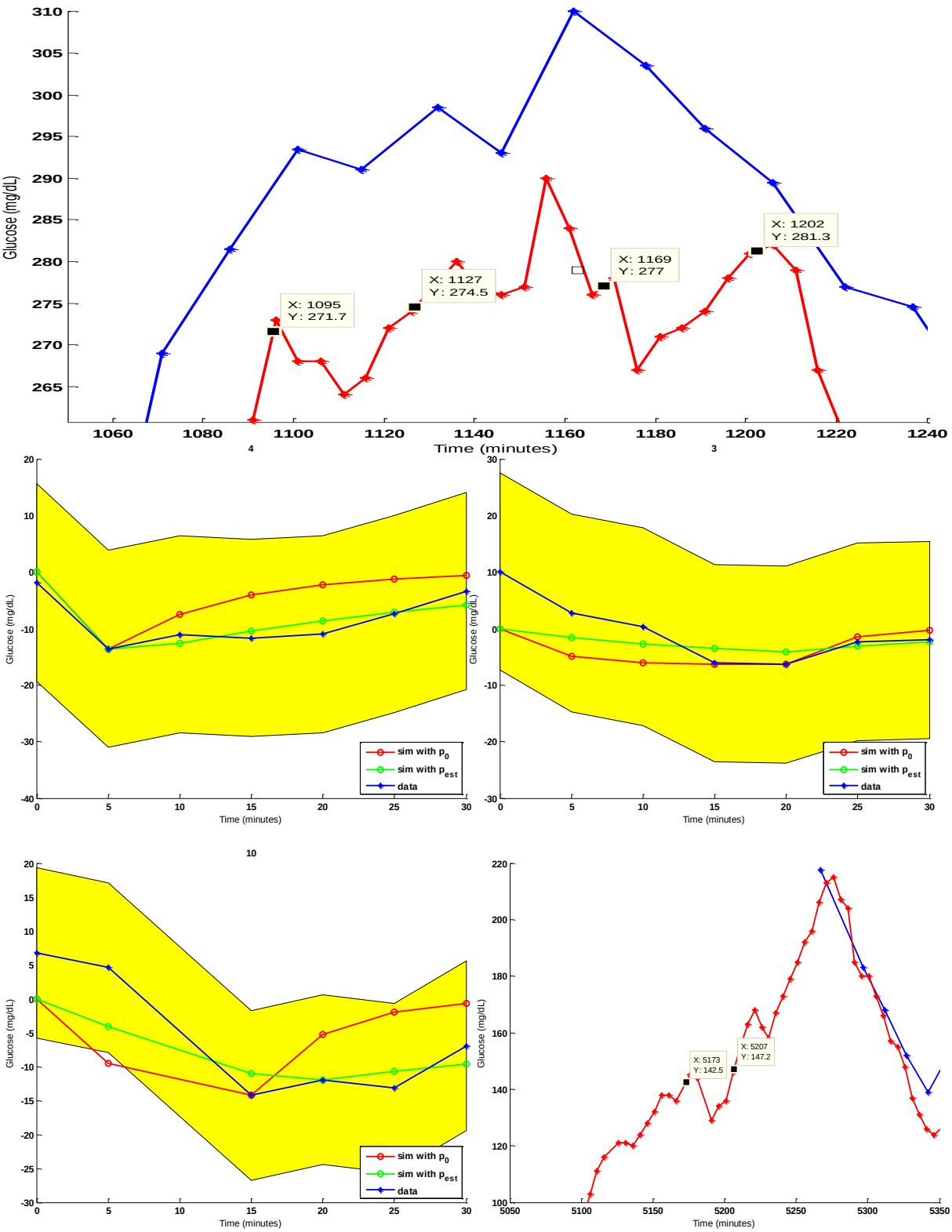

Figure 5.6 *Losses of sensitivity that gave bad estimation precision for the parameters F, D and τ.*

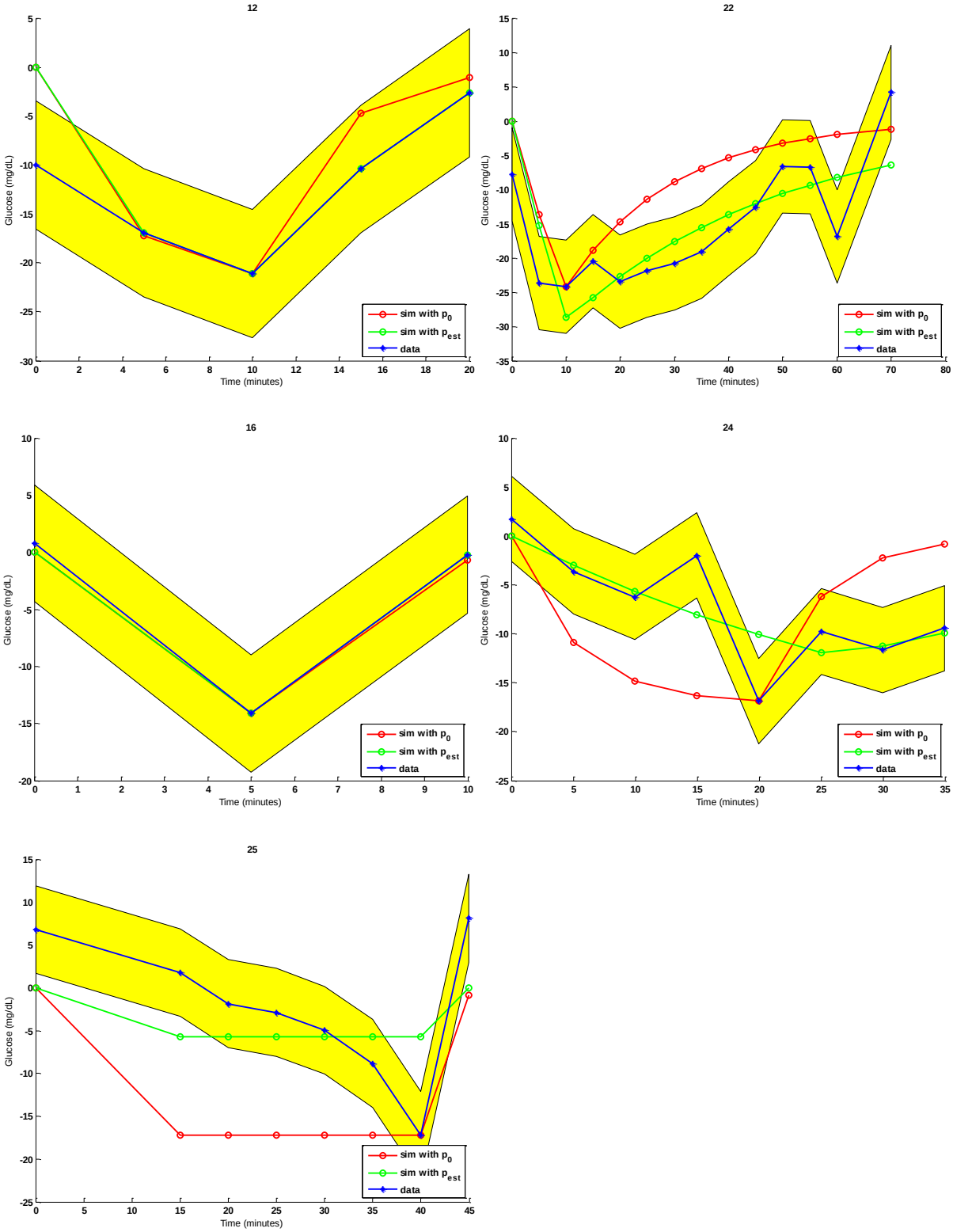

Figure 5.7 *Losses of sensitivity that are worth a careful evaluation.*

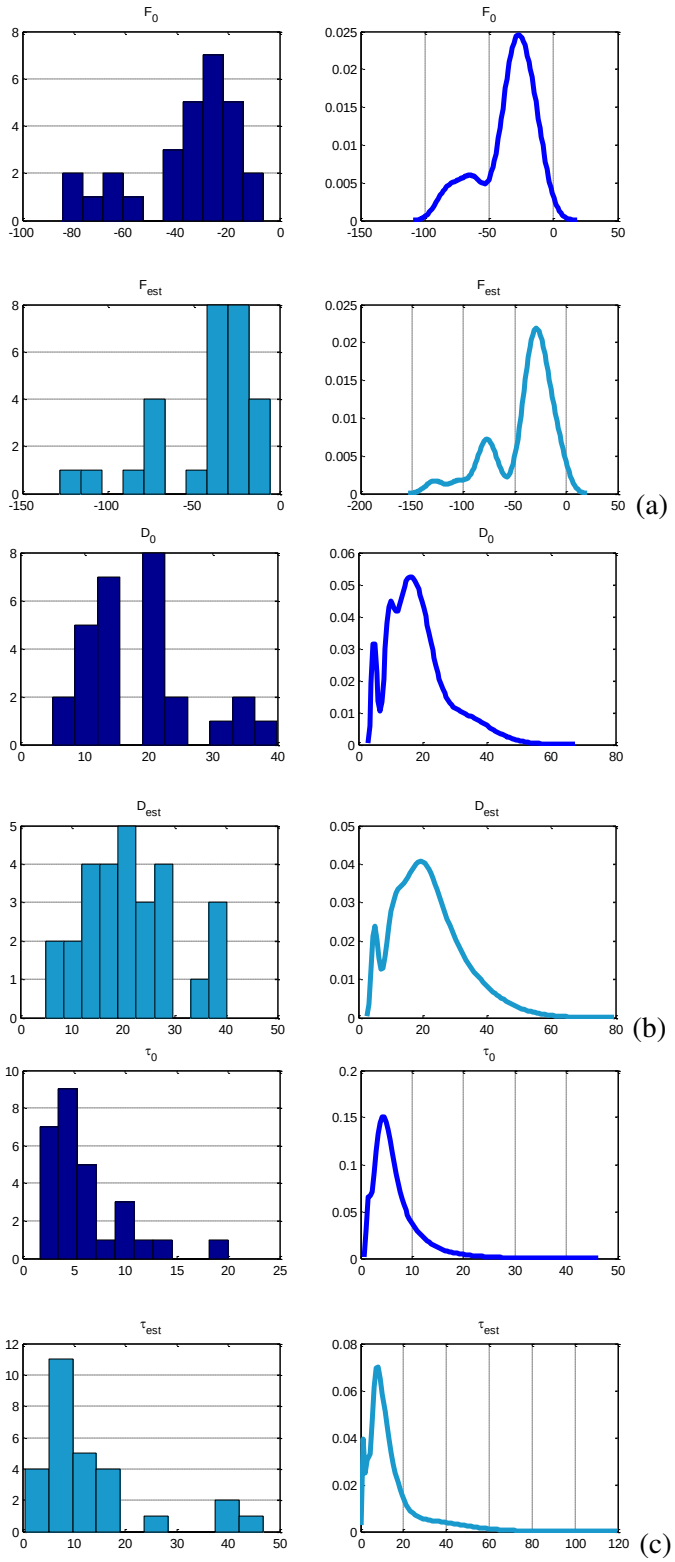

Figure 5.8 *Statistics of parameters F, D, τ: histogram and probability density function obtained via kernel density estimation for p_0 and $\hat{p}$. (a) F_0:*mean: -35.36, median: -29.76, st dev: 21.14*, F_{est}:*mean: -41.78, median: -33.08, st dev: 30.3*; (b) D_0:*mean: 18.43, median: 17.5, st dev: 8.79*, D_{est}:*mean: 21.33, median: 20.56, st dev: 9.36*; (c) τ_0:*mean: 6.46, median: 5, st dev: 3.91*, τ_{est}:*mean: 13.46, median: 9.41, st dev: 11.41.

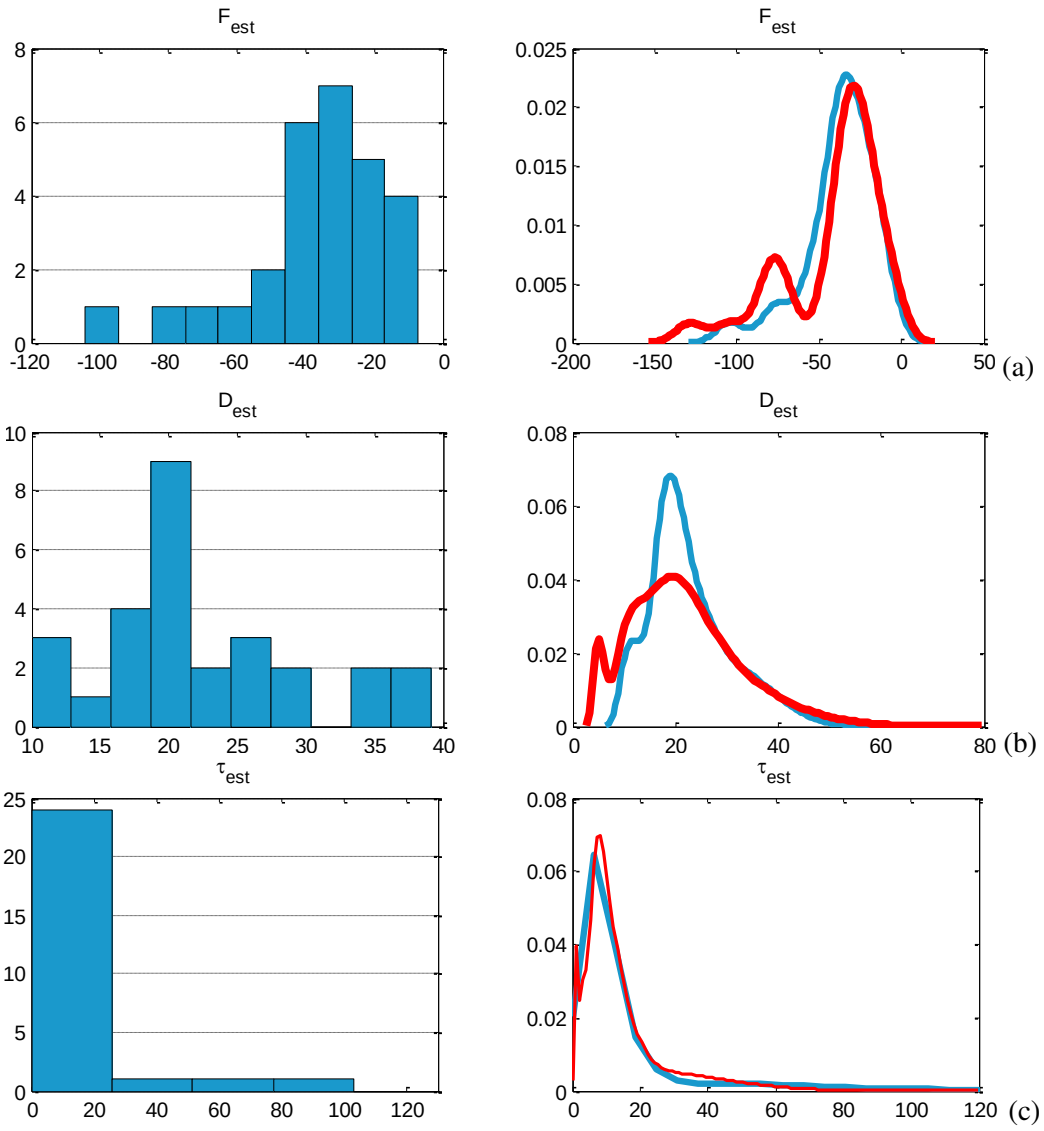

Figure 5.9 *Robustness of the estimation of model parameters to the initial guess. The red lines represent the probability density function of estimated parameters as discussed in Section 5.3.1 and shown in Figure 5.8.*

small sample. This matches our assumption in Section 5.3.

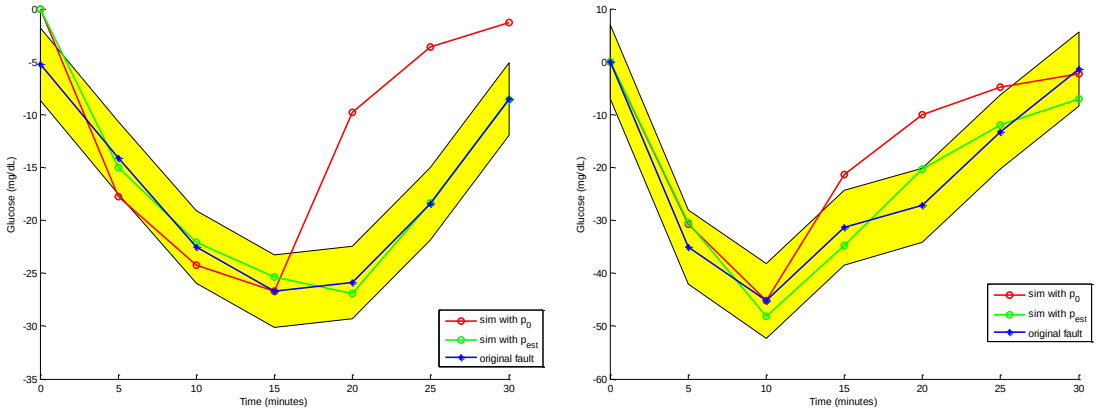

Figure 5.10 *Simulating two losses of sensitivity with the discussed model. The yellow area highlights the $\pm 2 \cdot$ confidence interval, the blue line represents the isolated failure from the real CGM data, the green line is the result with the best estimation of the parameters $\hat{p}$. The red line shows the simulated signal with the initial guess p_0, defined in Section 5.3.*

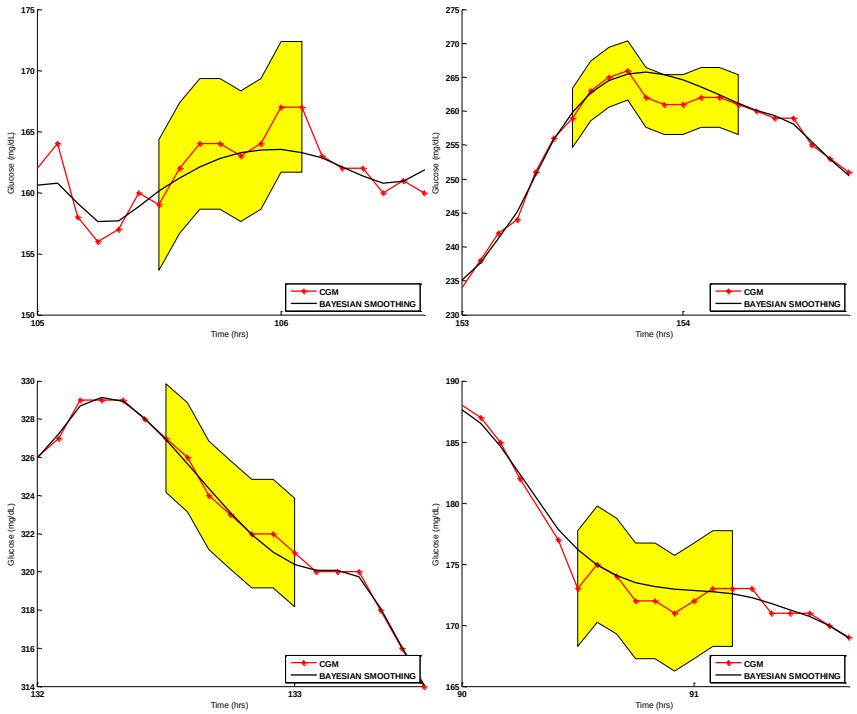

Figure 5.11 *The red lines show pieces of CGM signal with no failures, the black lines show the result for the bayesian smoothing obtained as described in Section 5.4, the yellow area highlights the $\pm 2 \cdot$ confidence interval.*

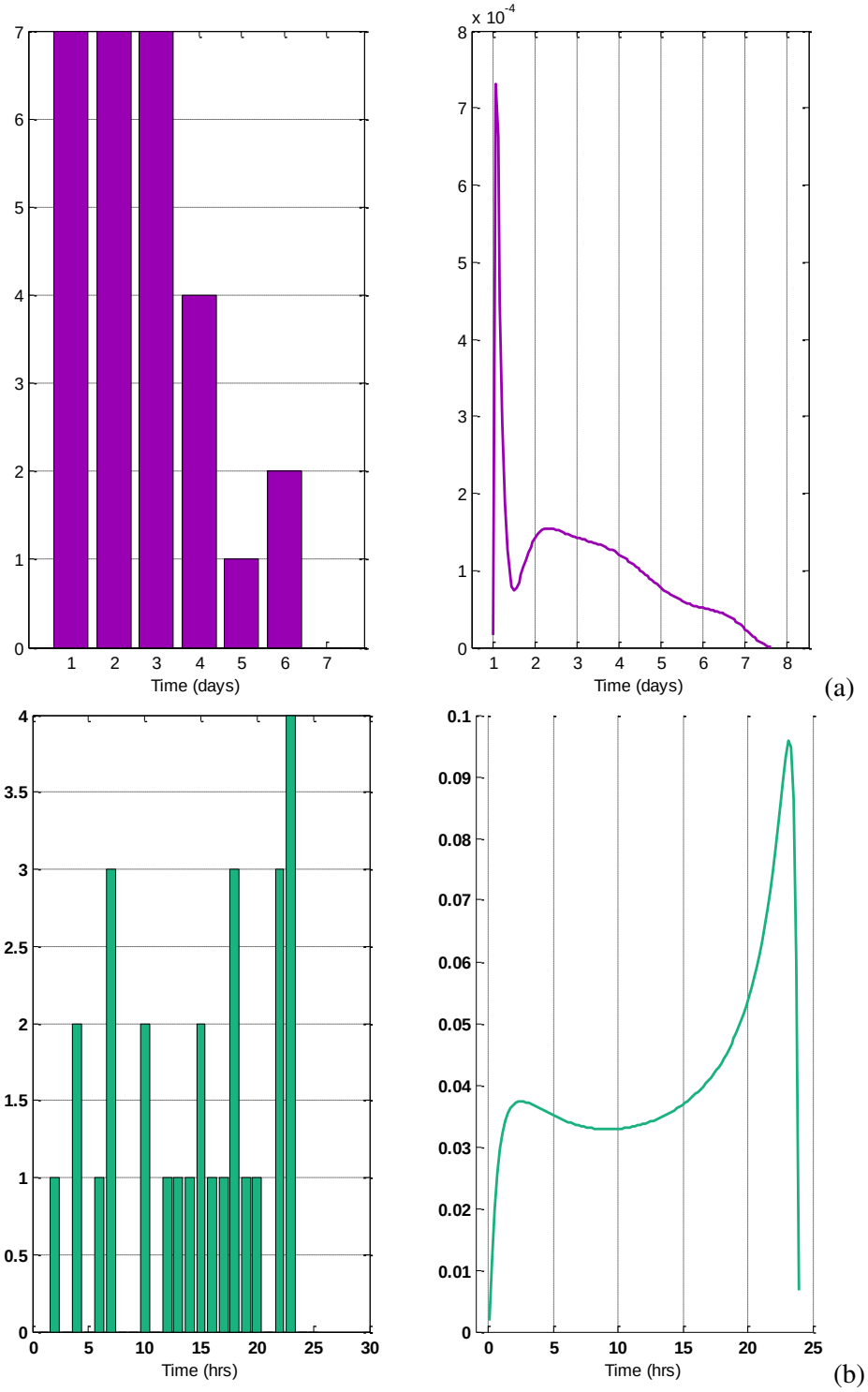

Figure 5.12 *(a): Distribution of losses of sensitivity over the several trial days. Left panel: histogram;* mean: 2.1367, stdev: 1.5519, median: 2.0259. *Right panel: probability density function estimated via kernel density estimation. (b): Distribution of losses of sensitivity over 24 hours. Left panel: histogram;* mean: 14.0718, st dev: 6.7086, median: 14.9315. *Right panel: probability density function estimated via kernel density estimation approach.*

6

Simulation of CGM faults

In the previous chapters we have shown how to simulate three of the most common failures one can detect in CGM real data. In this chapter, we show the results of the simulated failures, and add them to glycemic profiles obtained with the Simulator GIM. Testing control algorithms needs to cope with the most common failures one can find in CGM real data, hence we provide simulation tools that can be embedded with the simulated sensor block of the Simulator GIM.

6.1 Dalla Man *et al.* model

One of the most important application of CGM sensors is the Artificial Pancreas. The development of the Artificial Pancreas was largely enhanced by the Simulator of the human metabolism, i.e. the Glucose-Insulin Model (GIM) [16, 17]. This software realizes *in silico* mathematical models for both the diabetic patient and hardware components that take part in the closed loop control of glycemia in the Artificial Pancreas, i.e. the CGM sensor and the insulin pump. GIM is used by the researchers in order to develop and validate control algorithms, which saves time and money. In fact, this software was approved by Food and Drug Administration, the agency of the USA responsible for regulation and supervision of food and drug, as a substitute for animal trials. Hence, since 2008 control algorithms can be tested directly on human beings with no intermediate steps.

6.2 Simulation of disconnections

Exploiting the model described in Chapter 3, we discuss in this Section the results of a disconnections' simulation over 100 of 7-days lasting signals.

Figure 6.2 shows the statistical analysis of both the simulated disconnections and the real ones. For what concerns failures' duration, we can see from the histogram in the Figure (a) that the estimated $\hat{\beta}$ chosen in Section 3.3.2 gives a distribution of simulated disconnections similar

to the real one.

Panel (b) and (c) of Figure 6.2 show the probability density function obtained via kernel density estimation for failures' occurances during the 24 hours and sensor life. From these results, we can see that while for the 24 hours period we obtain a probability density function similar to the real one, for the 7days period this does not happen. Infact, we used the revised probability $\hat{\alpha}$, discussed in Section 3.5.3, but this is not a proper choice, since the probability for a failure to happen at one specific hour of the day is not independent from the probability for a failure to happen in one specific day of sensor life. Moreover, the probability density function estimated in Section 3.5.1 describes failures' occurances during sensor life, regardless of the real hour of the day.

6.3 Simulation of invalid outputs

As previously done for disconnections, we are here simulating invalid outputs as discussed in Section 4.4. We show the results for a simulation of 100 7-days lasting signals.

Figure 6.3 (a) shows the two histograms for simulated (left panel) and real (right panel) invalid outputs, with a focus in durations smaller than 60 samples. As discussed in Section 4.4, the information about durations was drawn from the sampling distribution of real failures, hence we can see that the two results are significantly similar.

Panel (b) and (c) of Figure 6.3 show the probability density function obtained via kernel density estimation for failures' occurances during the 24 hours and sensor life. In both cases, we see that the simulated distributions are similar to the real ones, demonstrating that our simulation procedure is correct.

6.4 Simulation of losses of sensitivity

Finally, we want to show that we could simulate losses of sensitivity as well. In order to choose the parameters F, D and τ, we used the statistical information of the estimated parameters. Figure 6.4 shows that we obtained simulated probability density functions of the simulated parameters similar to the real ones.

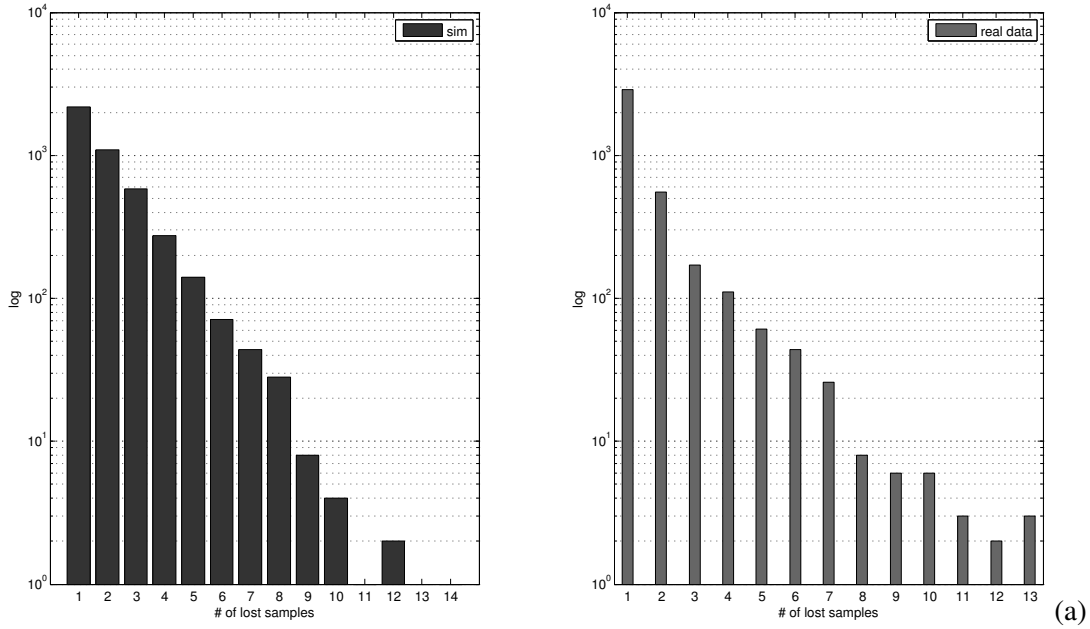

Figure 6.1 *(a) Left panel: durations' distribution of simulated disconnections. Right panel: durations' distribution of detected disconnections. (b) The distribution of simulated disconnections over the 24 hours (black curve) is very close of the real distribution (grey curve). (c) The distribution of simulated disconnections in the several days (black curve) is different from the real one (grey curve).*

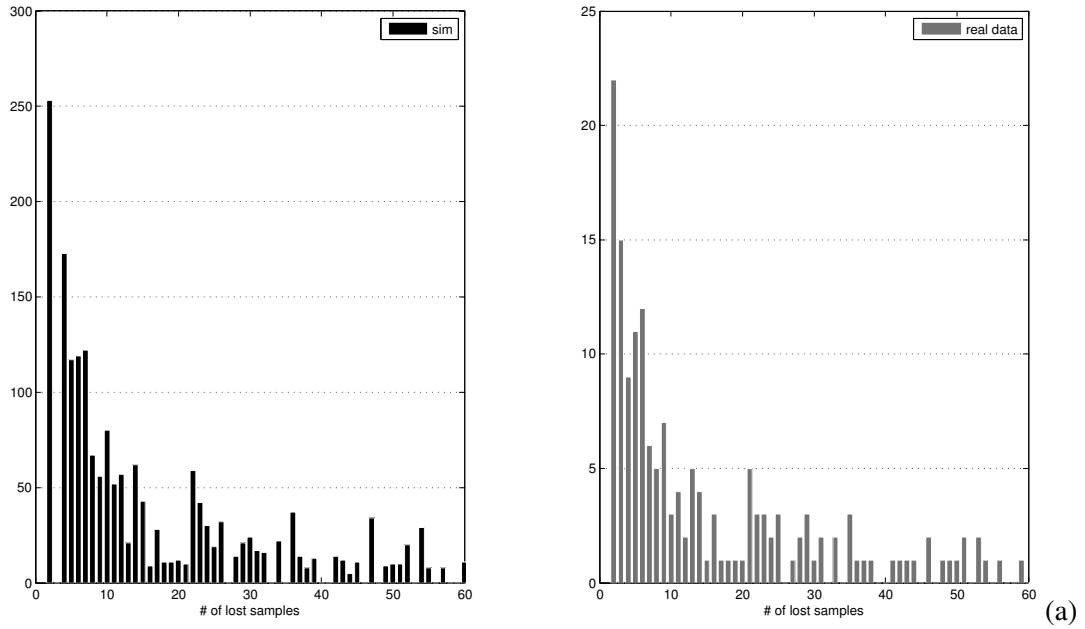

Figure 6.2 *(a) Left panel: durations' distribution of simulated invalid outputs. Right panel: durations' distribution of detected invalid outputs. (b)-(c) In both cases, the distribution of simulated invalid outputs over the 24 hours and the several days (black curve) is very close of the real distribution (grey curve).*

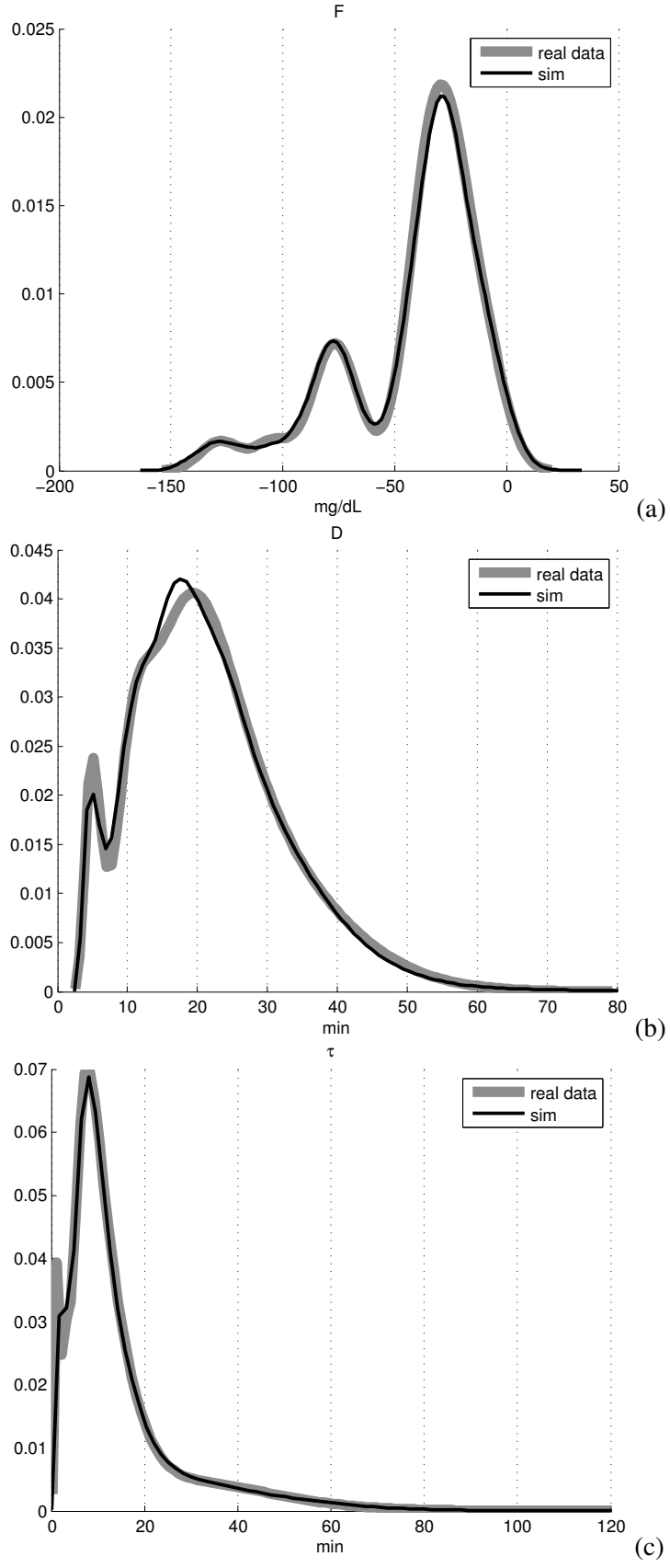

Figure 6.3 *Probability density function of simulated parameters F, D and τ compared to the real ones.*

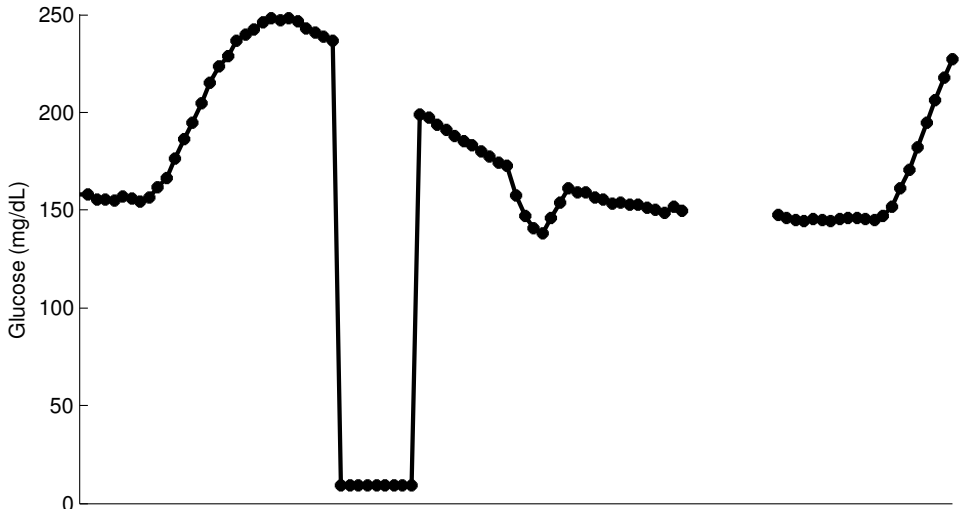

Figure 6.4 *Simulation of an invalid output, a loss of sensitivity and a disconnection on a virtual diabetic patient.*

6.5 Simulated failures applied to simulated CGM profile

Our purpose is to improve the simulated sensor block in the GIM simulator. Hence, adding the simulated failures to the simulated glycemic profiles, we can realize CGM profiles more similar to the real ones, so that robustness tests of control algorithms are more reliable.

Figure 6.5 an example of simulated diabetic (type-1) patient, and the scenario is:

- breakfast at 7 a.m. with 40 g of carbohydrates;
- lunch at 1 p.m. with 70 g of carbohydrates;
- dinner at 8 p.m with 80 g of carbohydrates.

7
Conclusions

CGM sensors are useful devices that supply several advantages and allow the development of important applications for diabetes management, such as the Artificial Pancreas. In order to test these applications, it is often used a physiological simulator of type-1 diabetic patient, that provides CGM simulated data for virtual patients. Nevertheless, these simulated profiles are not provided with the common failures we find instead in the real CGM signals (Dexcom® in this thesis), such as those we discussed in Chapters 3, 4 and 5. The closer simulated profiles are to the real ones, the more reliable are the testing results of these applications.

An investigation of the available data set led us to identify three main kinds of failures. The first one, we called *disconnection*, consists of the loss of at least one sample during the transmission of the signal between transmitter and receiver. We proposed and validated a two-state markov model for this failure. The same model did not work for the second kind of failure, which is an 'error code' displayed by the receiver, called *invalid output*. The third failure we discussed is the *loss of sensitivity*, which was modelled as a step function filtered by a first order system. We could simulate disconnections and losses of sensitivity and add the result at the output signal of the simulator, in order to obtain more realistic CGM profiles. For invalid outputs, we had to draw information from the empiric distribution since the model was not appropriate.

For what concerns disconnections, we obtained a simulation tool that is ready for use. Losses of sensitivity as well were described and simulated with a proper model, but still we can emphasize some open issues where there is substantial room for improvement:

1. failures' visual inspection is biased by the arbitrariness of the choice of starting and ending points;

2. different interpolation techniques should be investigated, other than linear interpolation and bayesian smoothing, since this step of the isolation procedure determines the shape of the failure;

3. only a small amount of losses of sensitivity were found, hence a larger data set should

be exploited in order to make our model more robust and statistically analyze time occurances.

Lastly, the model proposed for invalid outputs did not satisfy our validation criteria, hence we suggest two possible ways:

1. distinguishing between long and short-lasting invalid outputs, and modelling them separately;

2. testing a two-exponential model to describe both long and short-lasting invalid outputs.

Sharing information about ‘error codes’ with manufacturing companies might be useful.

A

Kernel Density Estimation

The objective of many investigation is to estimate the probability density function (pdf), $f(x)$, from a sample of observation $x_1, x_2, \cdots, x_n$.
The *parametric* approach for estimating $f(x)$ is to assume that $f(x)$ is a member of some parametric family of distributions, e.g. $N(\mu, \sigma^2)$, and then to estimate the parameters of the assumed distribution from the data. This approach has advantages as long as the distributional assumption is correct, or at least is not seriously wrong. The main disadvantage of the parametric approach is lack of flexibility. Each parametric family of distributions imposes restrictions on the shapes that $f(x)$ can have. For example the density function of the normal distribution is symmetrical and bell-shaped, and therefore is unsuitable for representing skewed densities or bimodal densities.

Methods that attempt to estimate the density directly from the data without assuming a particular form for the underlying distribution are called *non-parametric*. The simplest form of non-parametric estimation is the histogram, but it has several drawbacks, such as:

- the discontinuities of the estimate are an artifact of the chosen bin locations;
- the density estimate depends on the starting position of the bins.

Nevertheless, the histogram is useful for quick visualizations.

Kernel density estimation helps dealing with the two drawbacks we have just discussed. From the definition of the pdf, $f(x)$, of a random variable, X, one has that

$$P(x-h<X<x+h)=\int_{x-h}^{x+h} f(t)dt \approx 2hf(x)$$

and hence

$$f(x) \approx \frac{1}{2h} P(x-h<X<x+h) \tag{A.1}$$

The probability in A.1 can be estimated:

$$\hat{f}(x) = \frac{1}{2h} \frac{\text{number of observation in}(x-h, x+h)}{n} \tag{A.2}$$

and A.2 can be represented this way as well

$$\hat{f}(x) = \frac{1}{n}\sum_{i=1}^{n} w(x - x_i, h), \tag{A.3}$$

where $x_1, x_2, \cdots x_n$ are the realizations of the random variable and

$$w(t,h) = \begin{cases} \frac{1}{2h}, & \text{for } |t| < h \\ 0, & \text{otherwise} \end{cases}$$

The function defined in A.3 has the properties of a pdf, i.e. $\hat{f}(x)$ is non-negative for all x and the area between the x-axis and $\hat{f}(x)$ is equal to one. One way to interpret A.3 is to imagine that a rectangle (height $\frac{1}{2h}$ and width $2h$) is placed over each observed point on the x-axis. The estimate of the pdf at a given point is $\frac{1}{n}$ times the sum of the heights of all the rectangles that cover the point. By increasing h one increases the width of each rectangle and thereby increases the degree of smoothing.

Instead of rectangles, other weighting functions can be used, e.g. triangles:

$$w(t,h) = \begin{cases} \frac{1}{h}(1 - \frac{|t|}{h}), & \text{for } |t| < h \\ 0, & \text{otherwise} \end{cases}$$

Using triangles in A.3 once again makes $\hat{f}(x)$ a pdf, and increasing h increases the degree of smoothing here too.

Another weighting function is the Gaussian:

$$w(t,h) = \frac{1}{\sqrt{2\pi}} e^{-t^2/2h^2}, \qquad -\infty < t < \infty$$

In this case as well, increasing h implies a more regular $\hat{f}(x)$.

All the weighting functions $w(t,h)$ are of the form

$$w(t,h) = \frac{1}{h}K(\frac{t}{h}), \tag{A.4}$$

where K is a function of the variable t and is called *kernel*. A kernel is a standardized weighting function, namely the weighting function with $h = 1$. The kernel determines the shape of the weighting function. The parameter h is called the *bandwidth* or *smoothing constant*. It determines the amount of smoothing applied in estimating $f(x)$, i.e. the wider h is, the smoother the estimate $\hat{f}(x)$. For $h \to 0$, the kernel approaches a Dirac delta function, and $\hat{f}(x)$ approaches

the true density. However, in practice we have a finite number of points, so h cannot be made arbitrarily small, since the density estimate $\hat{f}(x)$ would then degenerate to a set of impulses located at the training data points.

In general any function having the following properties can be used as a kernel:

(a)

$$\int K(z)dz = 1$$

(b)

$$\int zK(z)dz = 0$$

(c)

$$\int z^2K(z)dz := k_2 < \infty$$

It follows that any symmetric pdf is a kernel. However, non-pdf kernels can also be used, e.g. kernels for which $K(z) < 0$ for some values of z. The latter type of kernels have the disadvantage that $\hat{f}(x)$ may be negative for some values of x.

Kernel estimation of pdfs is charactized by the kernel, K, which determines the shape of the weighting function, and the bandwidth, h, which determines the width of the weighting function and hence the amount of smoothing. The two components determine the properties of $\hat{f}(x)$.

B

Simulated losses of sensitivity

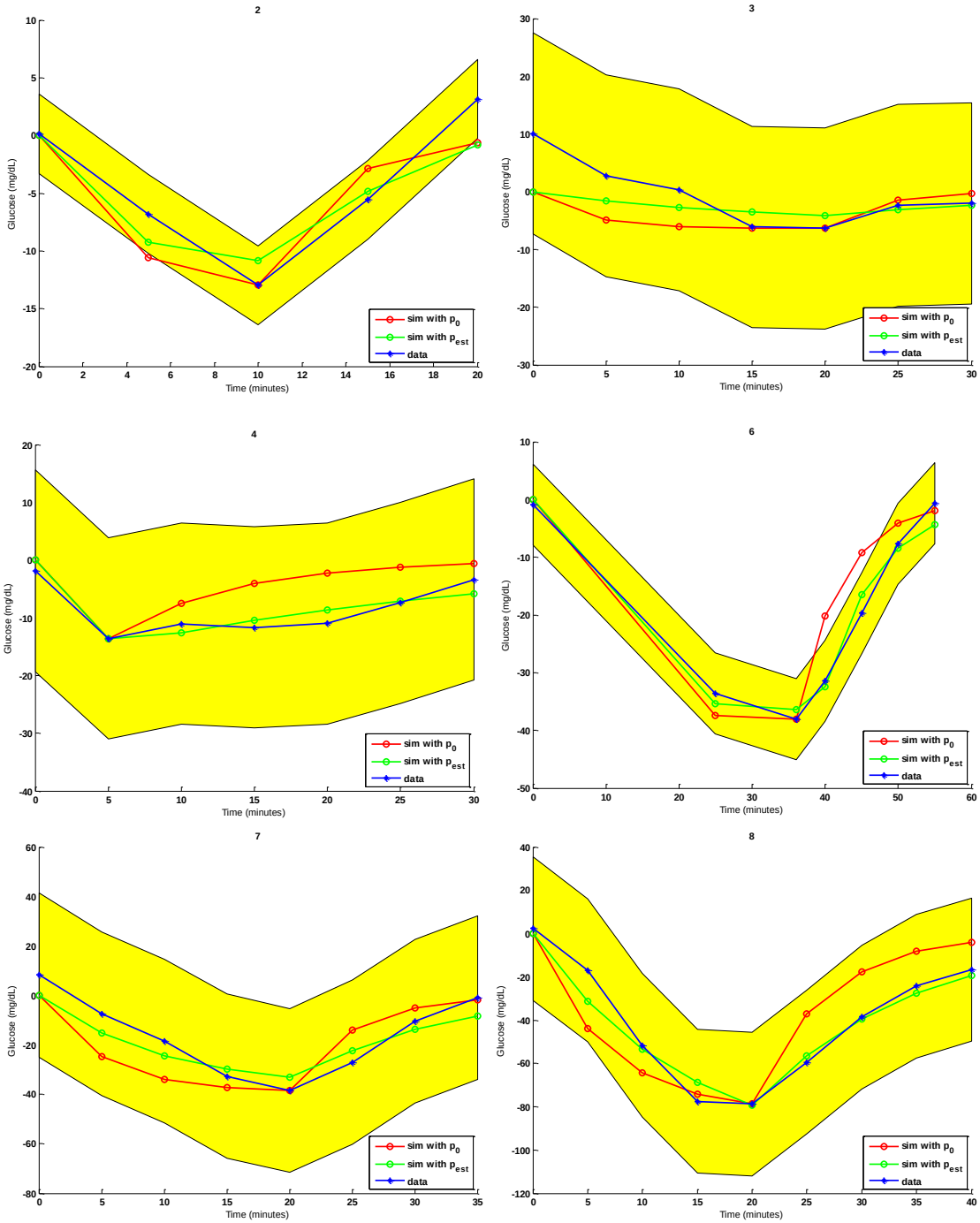

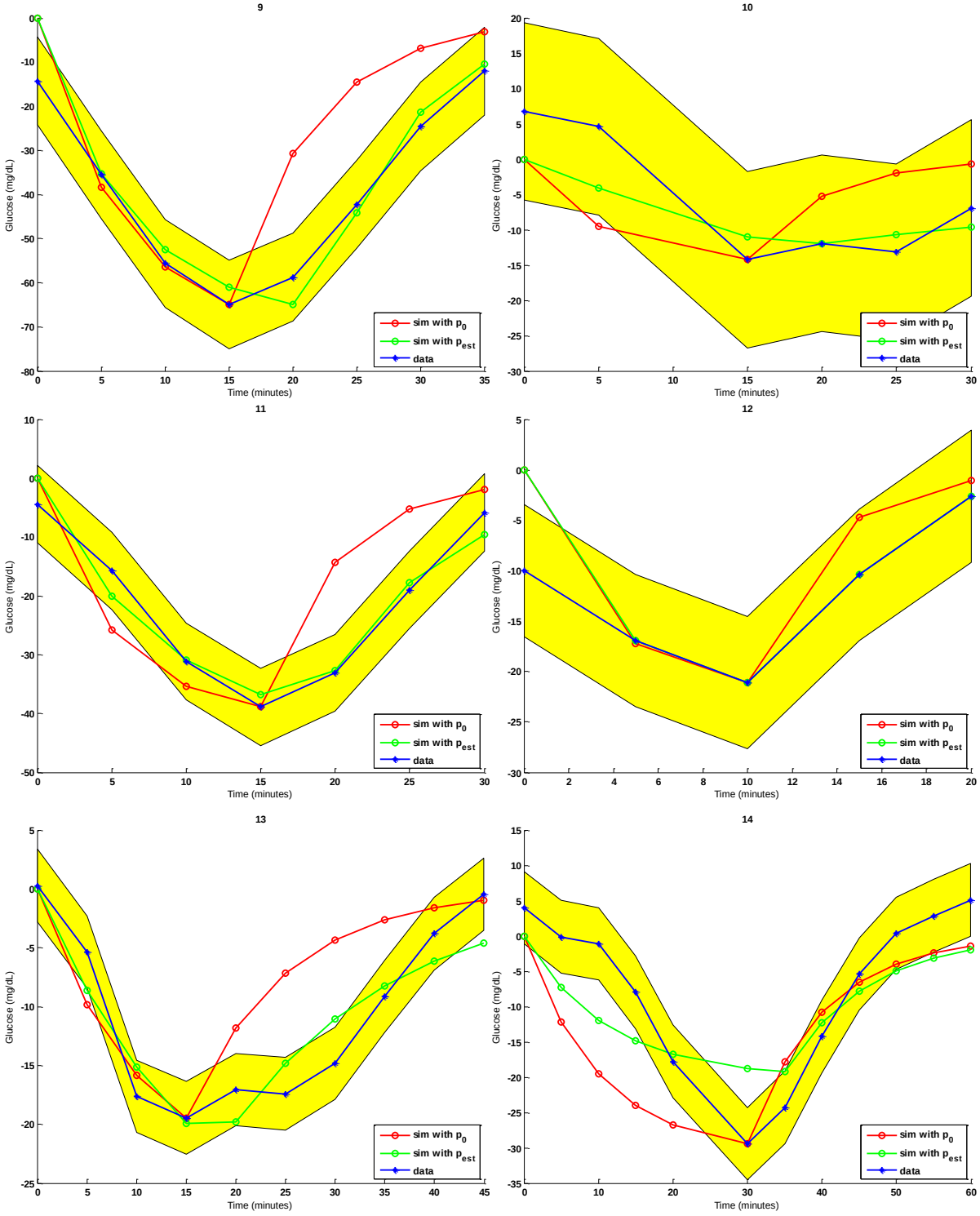
9
10
11
12
13
14
Glucose (mg/dL)
Time (minutes)
sim with p_0
sim with p_{est}
data

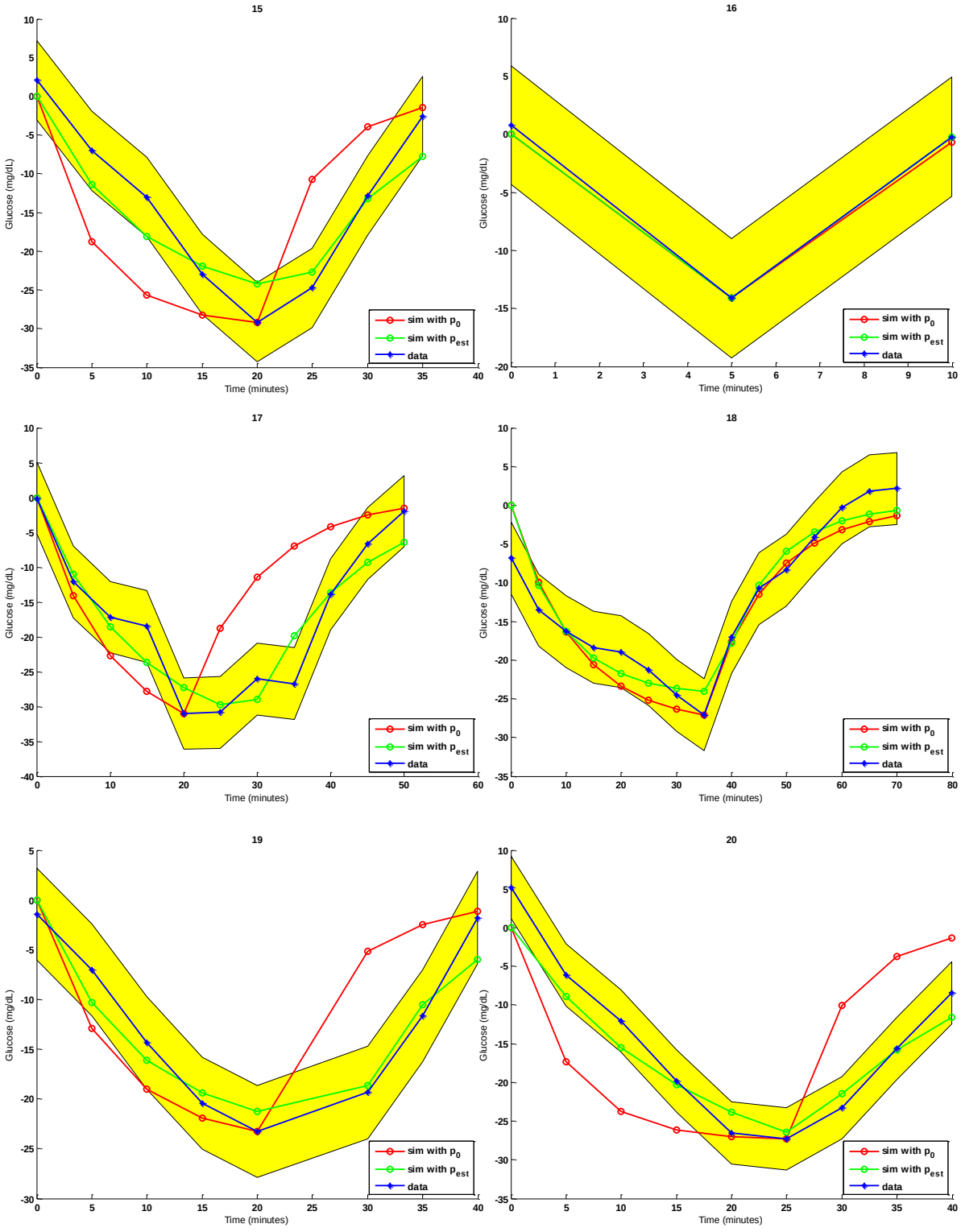
15
16
17
18
19
20
Glucose (mg/dL)
Time (minutes)
sim with p_0
sim with p_{est}
data

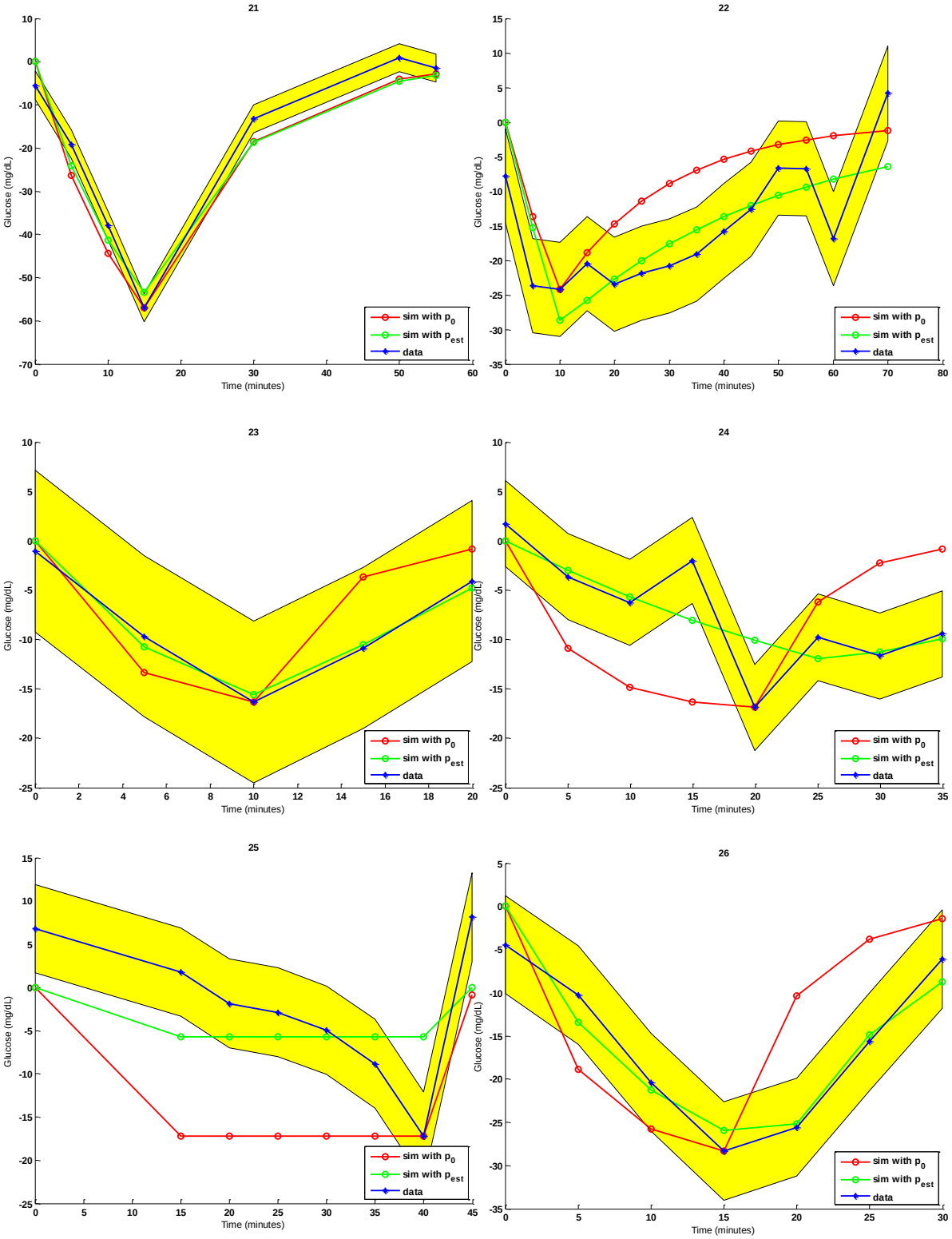
21
22
23
24
25
26
Glucose (mg/dL)
Time (minutes)
sim with p_0
sim with p_{est}
data

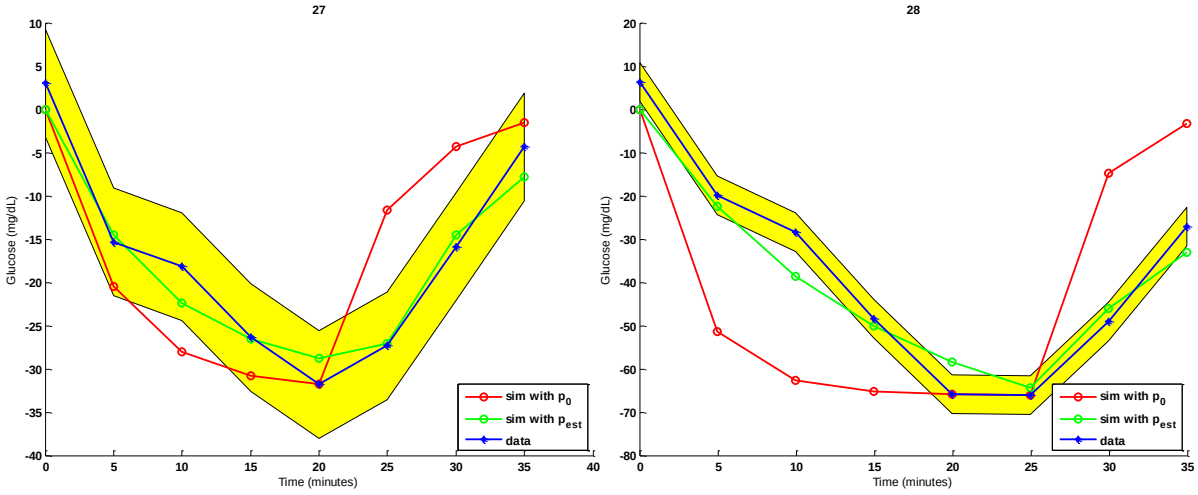

Figure B.1 *Simulated losses of sensitivity with the model. The yellow area highlights the confidence interval, the blue line represents the isolated failure from the real CGM data, the green line is the result with the best estimation of the parameters* $\hat{p}$.

Bibliography

[1] Apurv Kamath, Aarthi Mahalingam, James Brauker, 2010 Jan, *"Methods of Evaluating the Utility of Continuous Glucose Monitor Alerts"*, J Diabetes Sci Technol, 4(1), 57-66.

[2] Santhisagar Vaddiraju, Diane J. Burgess, Ioannis Tomazos, Faquir C. Jain, Fotios Papadimitrakopoulos, 2010 Nov, *"Technologies for Continuous Glucose Monitoring: Current Problems and Future Promises"*, J Diabetes Sci Technol, 4(6), 1540-1562.

[3] O. Amir, D. Weinstein, S. Zilberman, M. Less, D. Perl-Treves, H. Primack, A. Weinstein, E. Gabis, B. Fikhte, A. Karasik, 2007 Jul, *"Continuous Noninvasive Glucose Monitoring Technology Based on Occlusion Spectroscopy"*, J Diabetes Sci Technol, 1(4), 463-9.

[4] M. Mueller, M.S. Talary, L. Falco, O. De Feo, W.A. Stahel and A. Caduff, 2011 May, *"Data Processing for Noninvasive Continuous Glucose Monitoring with a Multisensor Device"*, J Diabetes Sci Technol, 5(3), 694-702.

[5] Jin Zhang, William Hodge, Cindy Hutnick, Xianbin Wang, 2011 Jan,*"Noninvasive Diagnostic Devices for Diabetes through Measuring Tear Glucose"*, J Diabetes Sci Technol, 5(1), 166-172.

[6] Lutz Heinemann, Carsten Benesch, J. Hans DeVries and the AP@home consortium, 2011 Nov, *"AP@home: A Novel European Approach to Bring the Artificial Pancreas Home"* , J Diabetes Sci Technol, 5(6), 1363-72.

[7] Stefano Ferri, Katsuhiro Kojima, Koji Sode, 2011 Sep,*"Review of Glucose Oxidases and Glucose Dehydrogenases: A Bird's Eye View of Glucose Sensing Enzymes"*, J Diabetes Sci Technol, 5(5), 1068-76.

[8] Giovanni Sparacino, Andrea Facchinetti and Claudio Cobelli, 2010 Jul, *"'Smart' Continuous Glucose Monitoring Sensors: On-Line Signal Processing Issues"*, Sensors, 10, 6751-72.

[9] Andrea Facchinetti, Giovanni Sparacino and Claudio Cobelli, 2010 Mar, *"An Online Self-Tunable Method to Denoise CGM Sensor Data"*, IEEE Transactions on Biomedical Engineering, 57(3), 634-41.

[10] Giuseppe De Nicolao, Giovanni Sparacino and Claudio Cobelli, 1997 May, *"Nonparametric Input Estimation in Physiological Systems: Problems, Methods, and Case Studies"*, Automatica, 33(5), 851-70.

[11] Boris Kovatchev and Marc Breton, 2010 Jan, *"The Accuracy of a New Real-Time Continuous Glucose Monitoring Algorithm: An Analysis"*, J Diabetes Sci Technol, 4(1), 119-122.

[12] Kristen L., Buddy D. Ratner and Natalie A. Wisniewski, 2011 May, *"Biomechanics of the Sensor-Tissure Interface–Effects of Motion, Pressure, and Design on Sensor Performance and Foreign Body Response–Part I: Theoretical Framework"*, J Diabetes Sci Technol, 5(3), 632-646.

[13] Kristen L., Buddy D. Ratner and Natalie A. Wisniewski, 2011 May, *"Biomechanics of the Sensor-Tissure Interface–Effects of Motion, Pressure, and Design on Sensor Performance and Foreign Body Response–Part II: Examples and Application"*, J Diabetes Sci Technol, 5(3), 647-656.

[14] Breton, Patek, Farret, Place, Demartini, Brown, Anderson, Kovatchev, Renard, 2011 Feb 16-19,*"Safety supervision system: first clinical trials. Proceedings of the Fourth Advanced Technologies and Treatments for Diabetes Annual Meeting"*, London, UK, Diabetes Technol Ther. 2011; 13(2), 176.

[15] Renard, Farret, Place, Cobelli, Kovatchev, Breton, 2010 Sep 20-24,*"Closed-loop insulin delivery using subcutaneous infusion and glucose sensing, and equipped with a dedicated safety supervision algorithm, improves safety of glucose control in type 1 diabetes"*, Proceedings of the 46th Annual Meeting of the European Association for the Study of Diabetes; Stockholm, Sweden.

[16] Chiara Dalla Man, Robert A. Rizza, and Claudio Cobelli, 2007 Oct, *"Meal Simulation Model of the Glucose-Insulin System"*, IEEE Transactions on Biomedical Engineering, 54(10), 1740-49.

[17] Chiara Dalla Man, Davide M. Raimondo, Robert A. Rizza, and Claudio Cobelli, 2007 May, *"GIM, Simulation Software of Meal Glucose-Insulin Model"*, J Diabetes Sci Technol 2007, 1(3), 323-330.

[18] *http://www.biovotion.com/*

[19] *http://www.medcompare.com/*

[20] *http://www.menarini.com/*

[21] *http://www.medtronicdiabetes.net/products/guardiancgm*

[22] *http://www.abbottdiabetescare.com*

[23] *http://www.dexcom.com/seven-plus*

[24] *http://www.c8medisensors.com/*

[25] *http://www.apathome.eu/*